

QCD Analysis of Polarized Deep Inelastic Scattering Data and Parton Distributions

Johannes Blümlein and Helmut Böttcher

Deutsches Elektronen Synchrotron, DESY

Platanenallee 6, D-15738 Zeuthen, Germany

Abstract

A QCD analysis of the world data on polarized deep inelastic scattering is presented in leading and next-to-leading order. New parameterizations are derived for the quark and gluon distributions for the kinematic range $x \in [10^{-9}, 1]$, $Q^2 \in [1, 10^6] \text{ GeV}^2$. The extrapolation far outside the domain of the current measurements is given both to allow for applications at higher values of Q^2 and to be able to calculate integral properties of the present distributions. The values of Λ_{QCD} and $\alpha_s(M_z)$ are determined. Emphasis is put on the derivation of the fully correlated 1σ error bands for these distributions, which are also given in terms of parameterizations and are directly applicable to determine experimental errors of other polarized observables. The impact of the variation of both the renormalization and factorization scales on the value of α_s is studied. Finally we perform a factorization-scheme invariant QCD analysis based on the observables $g_1(x, Q^2)$ and $dg_1(x, Q^2)/d\log(Q^2)$ in next-to-leading order, which is compared to the standard analysis. A series of low moments of parton densities, accounting for error correlation, are given to allow for comparison with results from lattice simulations.

1 Introduction

The nature of the short-distance structure of polarized nucleons is one of the central questions of present day hadron physics. Nucleons are composite fermions and their spin should be obtained as a superposition of the spins and angular momenta of its constituents, the quarks and gluons. At large enough space-like 4-momentum transfers $-q^2 = Q^2$ and large energy transfer $\nu = 2p \cdot q/M$, with p and M the nucleon 4-momentum and mass, the QCD-improved parton model applies. A QCD analysis at leading twist level allows to determine the polarized parton densities and the QCD scale Λ_{QCD} up to next-to-leading order (NLO) [1–3]. The distribution functions derived can be used to calculate other leading twist hard scattering cross sections of polarized nucleons.

During the recent years the remarkable growth of deep inelastic scattering data off polarized targets [4–13] allows to perform a detailed analysis. Here the different systematic effects of the data have to be taken into account. Previous analyzes [14–16]¹ present parameterizations only for the central values of the parton distributions. It is, however, desirable to derive at the same time parameterizations of the polarized parton densities and those of their 1σ error, taking into account all error correlations being available. With these parameterizations at hand it becomes possible to give estimates on the uncertainty of the measurement of other hard scattering processes of polarized targets w.r.t. the knowledge of the parton densities. In the analysis the polarized parton distributions are first determined at a reference scale Q_0^2 . The aforementioned parameterizations are found evolving both the central values and their errors from this scale to all scales Q^2 of interest, which we choose as $1 \text{ GeV}^2 \leq Q^2 \leq 10^6 \text{ GeV}^2$ for $x = Q^2/2p \cdot q \in [10^{-9}, 1]$, and are given in form of fast and accurate grid interpolations.

Unlike the case in most of the previous analyzes the QCD analysis performed in the present paper determines the QCD-scale Λ_{QCD} along with the parameters of the parton densities at the initial scale Q_0^2 . Moreover, positivity constraints are not imposed from the beginning but first left to the fit. A systematic investigation of the χ^2 -profiles during the analysis showed, which of the parameters of the parton densities have enough sensitivity to be measured from the current polarized deep-inelastic scattering world data. In this context it turns out that the current inclusive data do not yet allow to pin down the flavor structure of the sea quarks. Therefore we are going to use flavor $SU(3)$ in the current analysis and leave a refinement to a further analysis including as well semi-inclusive data.² As the subsequent analysis shows, the small- x behavior of the parton densities cannot be reliably fixed using the current data. Special dynamical effects [20, 21] may be present at smaller values of $x \lesssim 5 \cdot 10^{-3}$ than currently probed, however, reliable estimates cannot be given at present due to the lack of calculations on higher order resummed corrections in this kinematic range. Therefore we present two sets of parameterizations which could be both accommodated to the present data.

The standard analysis is performed using the $\overline{\text{MS}}$ factorization and renormalization scheme. In this way two independent scales, μ_f^2 and μ_R^2 , are introduced into the parton densities. The observables, $g_1^p(x, Q^2)$ and $g_1^n(x, Q^2)$, are independent of these scales which leads to two associated (matrix-valued) renormalization group equations for the Wilson-coefficients and parton densities, which are the evolution equations. Referring to also other observables, as e.g. the slopes $\partial g_1^{p,n}(x, Q^2)/\partial \log Q^2$, it is possible to each order in the coupling constant $a_s = \alpha_s/(4\pi)$ to formulate **physical** evolution equations [2, 23] of observables itself, which removes the dependence on μ_f^2 . This method of analysis is conceptually of high interest in future analyzes, having

¹In [17] another factorization scheme is referred to. For a list of older parameterizations see [18].

²The latter analysis can only be performed if the relevant fragmentation functions are known, cf. [19].

precise measurements of the respective observables at the scale Q_0^2 at hand. Then the *only* parameter to be fitted is Λ_{QCD} . We also perform this factorization–scheme independent analysis in next-to-leading order to check the stability of the fitted values of Λ_{QCD} .

Currently the measurement of also the moments of polarized parton densities on the lattice become more precise [23–25]. Yet a series of systematic and algorithmic effects has to be studied in detail, but one may expect that direct comparison between the moments of parton densities being extracted out of the world data and the lattice results will be possible in the future. This comparison has to include the proper treatment of errors both on the side of the lattice calculations and the perturbative analysis. This usually includes correlated propagation of the experimental errors through the evolution equations. To allow for comparisons with results from lattice calculations we provide a set of lowest moments of parton densities and their combinations including their errors in the present analysis.

The paper is organized as follows. In sections 2 and 3 the standard and the factorization–scheme independent analyzes to next-to-leading order are described. A summary on the experimental data used in the present analysis is given in section 4. Section 5 contains the details on the parameterizations of the parton densities and that of their 1σ errors. In Section 6 the results of the standard and factorization–scheme independent analysis on the parton densities and their errors at the scale Q_0^2 as well as their evolution throughout the kinematic range of the parameterization $1 \leq Q^2 \leq 10^6 \text{ GeV}^2$ are presented and the respective values of Λ_{QCD} and $\alpha_s(M_Z^2)$ are given and are discussed w.r.t the choice of the renormalization and factorization scales. The covariance matrices of the parameters determined in the QCD fits are provided. In section 7 a series of values of the lower moments of the parton densities and their errors, suitable for comparisons with results of lattice simulations, are calculated. Section 8 contains the conclusions. An appendix provides informations on the numerical parameterization of different sets of polarized parton densities and their errors.

2 Standard Analysis

The twist–2 contributions to the structure function $g_1(x, Q^2)$ can be represented in terms of a MELLIN convolution of the polarized parton densities Δf_i and the coefficient functions ΔC_i^A by

$$g_1(x, Q^2) = \frac{1}{2} \sum_{j=1}^{N_f} e_j^2 \int_x^1 \frac{dz}{z} \left[\frac{1}{N_f} \Delta \Sigma \left(\frac{x}{z}, \mu_f^2 \right) \Delta C_q^S \left(z, \frac{Q^2}{\mu_f^2} \right) + \Delta G \left(\frac{x}{z}, \mu_f^2 \right) \right. \\ \left. \times \Delta C^G \left(z, \frac{Q^2}{\mu_f^2} \right) + \Delta q_j^{NS} \left(\frac{x}{z}, \mu_f^2 \right) \Delta C_q^{NS} \left(z, \frac{Q^2}{\mu_f^2} \right) \right], \quad (1)$$

where e_j denotes the charge of the j th quark flavor and N_f is the number of flavors. The scale μ_f denotes the factorization scale which is introduced to remove the collinear singularities from the partonic structure functions. In addition the above quantities are dependent on the renormalization scale μ_r of the strong coupling constant $a_s(\mu_r^2) = g_s^2(\mu_r^2)/(16\pi^2)$. The structure function $g_1(x, Q^2)$, as a physical observable, is independent of the choice of both scales. The parton densities and the coefficient functions are dependent on these scales and obey corresponding renormalization group equations.

The singlet and non–singlet parton densities which occur in Eq. (1) are expressed by the

individual flavor contributions as

$$\Delta\Sigma(z, \mu_f^2) = \sum_{i=1}^{N_f} \left[\Delta f_{q_i}(z, \mu_f^2) + \Delta f_{\bar{q}_i}(z, \mu_f^2) \right], \quad (2)$$

and

$$\Delta q_i^{NS}(z, \mu_f^2) = \Delta f_{q_i}(z, \mu_f^2) + \Delta f_{\bar{q}_i}(z, \mu_f^2) - \frac{1}{N_f} \Delta\Sigma(z, \mu_f^2), \quad (3)$$

respectively, where f_{q_i} denotes the polarized quark distribution of the i th flavor.

The running coupling constant is obtained as the solution of

$$\frac{da_s(\mu_r^2)}{d\log(\mu_r^2)} = -\beta_0 a_s^2(\mu_r^2) - \beta_1 a_s^3(\mu_r^2) + O(a_s^4), \quad (4)$$

where the coefficients of the β -function are given by

$$\begin{aligned} \beta_0 &= \frac{11}{3}C_A - \frac{4}{3}T_F N_f, \\ \beta_1 &= \frac{34}{3}C_A^2 - \frac{20}{3}C_A T_F N_f - 4C_F T_F N_f, \end{aligned} \quad (5)$$

in the $\overline{\text{MS}}$ -scheme. Here $C_A = 3, T_F = 1/2, C_F = 4/3$ and N_f denotes the number of active flavors. In the QCD fit to the data we extract $\Lambda_{\text{QCD}}^{(4)}$ and choose $N_f = 4$ in Eq. (5) whereas only the three light flavors are used to represent $g_1(x, Q^2)$, Eq. (1). The expression for $\Lambda_{\text{QCD}}^{\overline{\text{MS}}}$ is given by

$$\Lambda_{\text{QCD}}^{\overline{\text{MS}}} = \mu_r \exp \left\{ -\frac{1}{2} \left[\frac{1}{\beta_0 a_s(\mu_r^2)} - \frac{\beta_1}{\beta_0^2} \log \left(\frac{1}{\beta_0 a_s(\mu_r^2)} + \frac{\beta_1}{\beta_0} \right) \right] \right\}. \quad (6)$$

Subsequently we will also compare the values of a_s at the mass scale of the Z -boson, $a_s(M_Z^2)$. This is obtained matching the values of a_s at the charm- and bottom-quark threshold $M_c = 1.4 \text{ GeV}$, $M_b = 4.5 \text{ GeV}$ using Eq. (6) for the value of $\Lambda_{\text{QCD}}^{\overline{\text{MS}}}$.

The change of the parton densities with respect to the factorization scale $\mu_f^2 = Q^2$ is described by (matrix-valued) renormalization group equations, the evolution equations, which read

$$\frac{\partial \Delta f_{q_i}^{\text{NS}}(x, Q^2)}{\partial \log Q^2} = P_{NS}^-(x, a_s) \otimes \Delta f_{q_i}^{\text{NS}}(x, Q^2), \quad (7)$$

$$\frac{\partial}{\partial \log Q^2} \begin{pmatrix} \Delta\Sigma(x, Q^2) \\ \Delta G(x, Q^2) \end{pmatrix} = \mathbf{P}(x, a_s) \otimes \begin{pmatrix} \Delta\Sigma(x, Q^2) \\ \Delta G(x, Q^2) \end{pmatrix}, \quad (8)$$

with

$$P_{NS}^-(x, a_s) = a_s P_{NS}^{(0)}(x) + a_s^2 P_{NS}^{-(1)}(x) + \mathcal{O}(a_s^3), \quad (9)$$

$$\mathbf{P}(x, a_s) \equiv \begin{pmatrix} P_{qq}(x, Q^2) & P_{qg}(x, Q^2) \\ P_{gq}(x, Q^2) & P_{gg}(x, Q^2) \end{pmatrix} = a_s \mathbf{P}^{(0)}(x) + a_s^2 \mathbf{P}^{(1)}(x) + \mathcal{O}(a_s^3), \quad (10)$$

and \otimes the MELLIN convolution

$$[A \otimes B](x) = \int_0^1 dx_1 dx_2 \delta(x - x_1 x_2) A(x_1) B(x_2). \quad (11)$$

The polarized coefficient functions and anomalous dimensions were calculated in [1-3] to next-to-leading order.

The evolution equations (7,8) may be rewritten changing the evolution variable $\log(Q^2)$ into a_s using Eq. (4):

$$d \log(Q^2) = - \frac{da_s}{\beta_0 a_s^2 + \beta_1 a_s^3} . \quad (12)$$

We solve the evolution equations in MELLIN- N space. For this purpose a MELLIN-transformation

$$\mathbf{M}[f](N) = \int_0^1 dx x^{N-1} f(x), \quad N \in \mathbf{N} \quad (13)$$

of the equations is carried out under which the MELLIN convolution \otimes turns into the ordinary product. After the transformation was performed the argument N is analytically continued to the complex plane. The principle way of solution of the Eqs. (7,8) is described in the literature in detail, see [2, 27, 21], which we summarize briefly. For the non-singlet case the solution to NLO is given by

$$\Delta q_i^{\text{NS}}(N, a_s) = \left(\frac{a_s}{a_0} \right)^{-P_{\text{NS}}^{(0)}/\beta_0} \left[1 - \frac{1}{\beta_0} (a_s - a_0) \left(P_{\text{NS}}^{-(1)} - \frac{\beta_1}{\beta_0} P_{\text{NS}}^{(0)} \right) \right] \Delta q_i^{\text{NS}}(N, a_0) , \quad (14)$$

where $a_s = a_s(Q^2)$, $a_0 = a_s(Q_0^2)$. The singlet solution reads

$$\begin{pmatrix} \Delta \Sigma(N, a_s) \\ \Delta G(N, a_s) \end{pmatrix} = [\mathbf{1} + a_s \mathbf{U}_1(N)] \mathbf{L}(N, a_s, a_0) [\mathbf{1} - a_0 \mathbf{U}_1(N)] \begin{pmatrix} \Delta \Sigma(N, a_0) \\ \Delta G(N, a_0) \end{pmatrix} . \quad (15)$$

Here the leading order evolution matrix \mathbf{L} is given by

$$\mathbf{L}(a_s, a_0, N) = \mathbf{e}_-(N) \left(\frac{a_s}{a_0} \right)^{-r_-(N)} + \mathbf{e}_+(N) \left(\frac{a_s}{a_0} \right)^{-r_+(N)} , \quad (16)$$

with eigenvalues of the LO singlet evolution matrix

$$r_{\pm} = \frac{1}{\beta_0} \left[\text{tr}(\mathbf{P}^{(0)}) \pm \sqrt{\text{tr}(\mathbf{P}^{(0)})^2 - \det_2(\mathbf{P}^{(0)})} \right] \quad (17)$$

and the eigenvectors

$$\mathbf{e}_{\pm} = \frac{\mathbf{P}^{(0)}/\beta_0 - r_{\mp} \mathbf{1}}{r_{\pm} - r_{\mp}} . \quad (18)$$

The matrix $\mathbf{U}_1(N)$ is given by

$$\mathbf{U}_1(N) = -\mathbf{e}_- \mathbf{R}_1 \mathbf{e}_- - \mathbf{e}_+ \mathbf{R}_1 \mathbf{e}_+ + \frac{\mathbf{e}_+ \mathbf{R}_1 \mathbf{e}_-}{r_- - r_+ - 1} + \frac{\mathbf{e}_- \mathbf{R}_1 \mathbf{e}_+}{r_+ - r_- - 1} \quad (19)$$

with

$$\mathbf{R}_1 = [\mathbf{P}^{(1)} - (\beta_1/\beta_0) \mathbf{P}^{(0)}] / \beta_0 . \quad (20)$$

The input distributions $\Delta q_i^{\text{NS}}(N, a_0)$, $\Delta \Sigma(N, a_0)$ and $\Delta G(N, a_0)$, see section 5, are evolved to the scale Q^2 , respectively to the coupling $a_s(Q^2)$. The inverse MELLIN-transform to x -space

is performed by a contour integral in the complex plane around all singularities, which can be written as

$$f_{\text{TH}}(x) = \frac{1}{\pi} \int_0^\infty dz \operatorname{Im} \left[\exp(i\phi) x^{-c(z)} f_{\text{TH}}[c(z)] \right] \quad (21)$$

applying symmetry properties of the integrand. In practice an integral along the path $c(z) = c_1 + \rho[\cos(\phi) + i \sin(\phi)]$, with $c_1 = 1.1$, $\rho \geq 0$ and $\phi = (3/4)\pi$ can be used. The upper bound on ρ is to be chosen by sufficient numerical convergence of the integral (21). The theoretical prediction $f_{\text{TH}}(x)$ for the respective observables depends on the parameters of the parton distributions chosen at the starting scale Q_0^2 and on Λ_{QCD} . These parameters are determined by a fit to the data using the χ^2 -method, see section 6.

3 Scheme Invariant Evolution of Polarized Structure Functions

In the foregoing section we investigated the QCD evolution of the polarized structure function $g_1(x, Q^2)$ at the level of twist-2 using the conventional picture of the QCD improved parton model. This requires choices of the non-perturbative partonic input distributions at a starting scale Q_0^2 . One outcome of the analysis is that some of the distributions are still very difficult to determine by a fit to the polarized deep inelastic data. This particularly applies to the polarized gluon and sea-quark densities.

The scaling violations of deep inelastic structure functions, i.e. their Q^2 -behavior, are properties of observables, and do thus *not* depend on particular representations, as scheme-dependent decompositions, which occur applying the parton model. Instead referring to the latter one might wish to eliminate the scheme dependence as occurring due to mass factorization all together and describe the evolution of polarized structure functions based on *observables* only. As a consequence, no parton distributions would even emerge in this description, and choices of the parameterization of less constraint input densities can be avoided.³

Up to NLO the evolution of the structure function $g_1(x, Q^2)$ is described by one non-singlet (7) and the coupled singlet evolution equations (8). Instead of Eq. (7) one may use the scheme-invariant equation based on the non-singlet structure function $g_1^{\text{NS}}(x, Q^2)$

$$\frac{\partial g_1^{\text{NS}}(x, Q^2)}{\partial t} = K^{\text{NS}}(a, x) \otimes g_1^{\text{NS}}(x, Q^2) \quad (22)$$

with⁴

$$K^{\text{NS}}(a, x) = \frac{a}{2} \left\{ P_0^{\text{NS}}(x) + a \left[P_1^{\text{NS}}(x) - \frac{\beta_1}{\beta_0} P_0^{\text{NS}}(x) - \beta_0 c_{q,1}(x) \right] \right\}. \quad (23)$$

Here the evolution variable is chosen as

$$t = -\frac{2}{\beta_0} \ln \left(\frac{a_s(Q^2)}{a_s(Q_0^2)} \right). \quad (24)$$

³After having carried out the analysis projections onto the various parton-densities, including the gluon density, in *whatever* factorization scheme, the $\overline{\text{MS}}$ scheme or other schemes [22, 17], are possible including the respective experimental errors.

⁴Note that the splitting functions and coefficient functions are expressed in such a way that all evolution equations refer to logarithmic variations in Q^2 and $a(Q^2)$ is used as the coupling constant.

For the singlet–evolution two observables have to be selected to form the factorization–scheme invariant evolution equations. In case of the polarized structure functions a natural choice is to use the flavor–singlet part of $g_1(x, Q^2)$ and its partial derivation w.r.t. t .⁵ The singlet evolution equation reads (taking the MELLIN transform)

$$\frac{\partial}{\partial t} \begin{pmatrix} F_A^N \\ F_B^N \end{pmatrix} = -\frac{1}{4} \mathbf{K}_S^{g_1}(N) \begin{pmatrix} F_A^N \\ F_B^N \end{pmatrix} = -\frac{1}{4} \begin{pmatrix} K_{AA}^N & K_{AB}^N \\ K_{BA}^N & K_{BB}^N \end{pmatrix} \begin{pmatrix} F_A^N \\ F_B^N \end{pmatrix}, \quad (25)$$

with $F_A = g_1(N, Q^2)$, $F_B = \partial g_1(N, Q^2)/\partial t$. The **physical** evolution kernels are given in leading order by

$$\begin{aligned} K_{22}^{N(0)} &= 0, & K_{2d}^{N(0)} &= -4, \\ K_{d2}^{N(0)} &= \frac{1}{4} \left(\gamma_{qq}^{N(0)} \gamma_{gg}^{N(0)} - \gamma_{qg}^{N(0)} \gamma_{gq}^{N(0)} \right), & K_{dd}^{N(0)} &= \gamma_{qq}^{N(0)} + \gamma_{gg}^{N(0)}. \end{aligned} \quad (26)$$

In next-to-leading order they read

$$K_{22}^{N(1)} = 0, \quad (27)$$

$$K_{2d}^{N(1)} = 0, \quad (28)$$

$$\begin{aligned} K_{d2}^{N(1)} &= \frac{1}{4} \left[\gamma_{gg}^{N(0)} \gamma_{qq}^{N(1)} + \gamma_{gg}^{N(1)} \gamma_{qq}^{N(0)} - \gamma_{qg}^{N(1)} \gamma_{gq}^{N(0)} - \gamma_{qg}^{N(0)} \gamma_{gq}^{N(1)} \right] \\ &\quad - \frac{\beta_1}{2\beta_0} \left(\gamma_{qq}^{N(0)} \gamma_{gg}^{N(0)} - \gamma_{gq}^{N(0)} \gamma_{qg}^{N(0)} \right) + \frac{\beta_0}{2} C_{2,q}^{N(1)} \left(\gamma_{qq}^{N(0)} + \gamma_{gg}^{N(0)} - 2\beta_0 \right) \\ &\quad - \frac{\beta_0}{2} \frac{C_{2,g}^{N(1)}}{\gamma_{qg}^{N(0)}} \left[(\gamma_{qq}^{N(0)})^2 - \gamma_{qq}^{N(0)} \gamma_{gg}^{N(0)} + 2\gamma_{qg}^{N(0)} \gamma_{gq}^{N(0)} - 2\beta_0 \gamma_{qq}^{N(0)} \right] \\ &\quad - \frac{\beta_0}{2} \left(\gamma_{qq}^{N(1)} - \frac{\gamma_{qq}^{N(0)} \gamma_{qg}^{N(1)}}{\gamma_{qg}^{N(0)}} \right), \end{aligned} \quad (29)$$

$$\begin{aligned} K_{dd}^{N(1)} &= \gamma_{qq}^{N(1)} + \gamma_{gg}^{N(1)} - \frac{\beta_1}{\beta_0} \left(\gamma_{qq}^{N(0)} + \gamma_{gg}^{N(0)} \right) \\ &\quad - \frac{2\beta_0}{\gamma_{qg}^{N(0)}} \left[C_{2,g}^{N(1)} \left(\gamma_{qq}^{N(0)} - \gamma_{gg}^{N(0)} - 2\beta_0 \right) - \gamma_{qg}^{N(1)} \right] + 4\beta_0 C_{2,q}^{N(1)} - 2\beta_1. \end{aligned} \quad (30)$$

Here $\gamma_{ij}^{N(0,1)}$ denotes the polarized deep–inelastic anomalous dimensions

$$\gamma_{ij}(a, N) = \sum_{k=0}^{\infty} a^{k+1} \gamma_{i,j}^{(k)}(N), \quad (31)$$

$$\gamma_{ij}^{N(0,1)} = -2 \int_0^1 dz z^{N-1} P_{ij}^{(0,1)}(z), \quad (32)$$

⁵Evolution equations of this type have been discussed before in Ref. [2]. In the unpolarized case one may consider the pair $F_2(x, Q^2), F_L(x, Q^2)$ as well, which has been considered in detail in Ref. [23]. For similar approaches, partly derived only for the small- x domain, see [28]. Corresponding evolution equations for time–like virtualities, which describe fragmentation in a factorization–scheme invariant way, were given in [23].

and $C_{2,q(g)}^{N(1)}$ is the MELLIN-transform of the Wilson coefficients

$$C_{2,k}^{N(1)} = \int_0^1 dz z^{N-1} C_{2,k}^{(1)}(z) . \quad (33)$$

For this combination in next-to-leading order the evolution depends on two evolution kernels only.

The kernels K^{NS} and $\mathbf{K}_S^{g_1}$ are factorization scheme-invariant quantities. Their analytic structure in z -space is difficult to obtain due to the inverse MELLIN-convolutions of inverse coefficient functions being required. Already in the case of the inverse of the leading order splitting function $P_{gq}(z)$ a rather complicated expression is found [29]. Therefore we perform all computations in MELLIN- N space, where the physical evolution kernels are polynomials out of anomalous dimensions and coefficient functions. Their analytic continuation to complex values of N can be performed using the respective representations of harmonic sums at high numerical precision, cf. [30]. In the unpolarized case approximate representations were also obtained in [31].

The advantage of studying factorization-scheme invariant evolution equations both in the non-singlet and the singlet case is that the input distributions are observables. Although the present world statistics is too low, future high statistics measurements may provide accurate input densities $g_1(x, Q_0^2)$ and $dg_1(x, Q_0^2)/dt$. In this case the **only** parameter to be measured analyzing the scaling violations of $g_1(x, Q^2)$ is Λ_{QCD} . At present the solution of the physical evolution equations in the polarized case cannot yet take full advantage of the method, since the respective observables are not yet measured well enough at typical input scales Q_0^2 . This different formulation, however, leads to an alternative view on the data in extracting Λ_{QCD} , as different input densities, $g_1(x, Q_0^2)$ and $dg_1(x, Q_0^2)/dt$, are fitted as compared to $\Delta\Sigma(x, Q_0^2)$ and $\Delta G(x, Q_0^2)$ in the standard analysis. A comparison of the values of Λ_{QCD} obtained in both analyzes may indicate the stability of the determination of the QCD-parameter.

4 Data

The remarkable growth of experimental data on inclusive polarized deep inelastic scattering of leptons off nucleons over the last years allows to perform refined QCD analyzes of polarized structure functions in order to reveal the spin-dependent partonic structure of the nucleon. For the QCD analysis presented in the present paper the following data sets are used: the EMC proton data [4], the E142 neutron data [5], the HERMES neutron data [6], the E154 neutron data [7], the SMC proton and deuteron data [8], the E143 proton and deuteron data [9], the HERMES proton data [10], the E155 deuteron data [11], and the E155 proton data [12]⁶. The number of the published data points above $Q^2 = 1.0 \text{ GeV}^2$ for the different data sets are summarized in Table 1 for both the asymmetry data, i.e. g_1/F_1 or A_1 , and data on g_1 together with the x - and Q^2 -ranges for the different experiments.⁷ There are 435 data points for asymmetry data, a number which exceeds the number of data points for g_1 data by a factor of two. We therefore are utilizing the asymmetry data which are expected to give a better statistical accuracy.

The QCD fits are performed on the polarized structure function $g_1(x, Q^2)$ which has to be evaluated from the asymmetry data. Experimentally cross section asymmetries for longitudinally

⁶Earlier data from Ref. [13] are not considered.

⁷All corrections to the data are assumed to be carried out, including the QED radiative corrections [32, 33].

polarized lepton scattering off longitudinally polarized nucleons are measured

$$A_{||} = \frac{\sigma^{\uparrow\uparrow} - \sigma^{\uparrow\downarrow}}{\sigma^{\uparrow\uparrow} + \sigma^{\uparrow\downarrow}} . \quad (34)$$

The arrow-combination $\uparrow\uparrow(\uparrow\downarrow)$ denotes parallel(anti-parallel) spin orientation of the lepton and the nucleon. The ratio of structure functions g_1/F_1 and the longitudinal virtual photon asymmetry A_1 are related to $A_{||}$ by

$$\frac{g_1}{F_1} = \frac{1}{(1 + \gamma^2)} \left[\frac{A_{||}}{D} + (\gamma - \eta)A_2 \right] , \quad (35)$$

$$A_1 = \frac{A_{||}}{D} - \eta A_2 , \quad (36)$$

and the relation between g_1/F_1 and A_1 is

$$\frac{g_1}{F_1} = \frac{1}{(1 + \gamma^2)} [A_1 + \gamma A_2] . \quad (37)$$

Here A_2 is the transverse virtual photon asymmetry and

$$D = \frac{1 - (1 - y)\epsilon}{1 + \epsilon R(x, Q^2)} , \quad (38)$$

$$\epsilon = \frac{4(1 - y) - \gamma^2 y^2}{2y^2 + 4(1 - y) + \gamma^2 y^2} , \quad (39)$$

$$\gamma = \frac{2Mx}{\sqrt{Q^2}} , \quad (40)$$

$$\eta = \frac{\epsilon \gamma y}{1 - \epsilon(1 - y)} . \quad (41)$$

D denotes the virtual photon depolarization factor, ϵ , γ and η are kinematic factors, $y = Q^2/(Sx)$ is the Bjorken variable, with $S = M^2 + 2ME_e$, M the nucleon mass, E_e the electron energy in the target rest frame, and $R(x, Q^2) = \sigma_L/\sigma_T$. For $R(x, Q^2)$ the SLAC parameterization R_{1990} [34] is used by most of the experiments. At the time of the EMC experiment this parameterization was not available yet and R was assumed to be Q^2 independent. The SMC collaboration adopted a combination of R_{1990} (for $x > 0.12$) and a parameterization derived by the NMC collaboration [35] (for $x < 0.12$). In the E155 experiment a recent SLAC parameterization for R [36] was used. The changes in the data caused by using the different R parameterizations are not significant and stay within the experimental errors⁸.

The magnitude of A_2 has been measured by SMC [37], E154 [38], and E143 [9] and found to be small. To a good approximation its contribution to g_1/F_1 and A_1 which is being further suppressed by the kinematic factors γ and η can be neglected. Nevertheless, E143 and E154 have exploited their measurements, E155 has approximated this contribution by $g_2^{\text{WW}}(x, Q^2)$ through the Wandzura–Wilczek expression [39],⁹ which is calculated from the measured structure function $g_1(x, Q^2)$ in the approximation that twist-2 contributions are dominant:

$$g_2^{\text{WW}}(x, Q^2) = -g_1(x, Q^2) + \int_x^1 \frac{dz}{z} g_1(z, Q^2) . \quad (42)$$

⁸The EMC proton data, where the biggest impact is expected, change by a few percent only, see Ref. [15].

⁹Note that this relation holds also in the presence of quark- [40] and target-mass corrections [40, 41]. Related integral relations for twist-3 contributions and structure functions with electro-weak couplings were derived in Refs. [40, 42]. Recently these relations have been found to hold also for diffractive scattering, [43].

HERMES has accounted for the A_2 contribution to the proton data by using a fit based on existing measurements [10]. To obtain $g_1(x, Q^2)$ one has to multiply the ratio $g_1(x, Q^2)/F_1(x, Q^2)$ with the unpolarized structure function $F_1(x, Q^2)$ which can be calculated from the usually measured unpolarized structure function $F_2(x, Q^2)$ by

$$F_1(x, Q^2) = \frac{(1 + \gamma^2)}{2x(1 + R(x, Q^2))} F_2(x, Q^2) . \quad (43)$$

For all data sets we are using the SLAC $R_{1990}(x, Q^2)$ [34] and the NMC $F_2(x, Q^2)$ parameterization [44] to perform this calculation.

The data sets used contain both statistical and systematic errors except the SMC data set which is given with statistical errors only. It is known that the systematic errors are partly correlated which would lead to an overestimation of the errors when added in quadrature with the statistical ones and hence to a reduction of the χ^2 value in the minimization procedure. To treat all data sets on the same footing we decided to use the statistical errors only. However, we allow for a relative normalization shift between the different data sets within the normalization uncertainties quoted by the experiments. Thereby we are taking into account the main systematic uncertainties coming from the measurements of the luminosity and the beam and target polarization. The normalization shift for each data set enters as an additional term in the χ^2 -expression which then reads

$$\chi^2 = \sum_{i=1}^{n^{exp}} \left[\frac{(N_i - 1)^2}{(\Delta N_i)^2} + \sum_{j=1}^{n^{data}} \frac{(N_i g_{1,j}^{data} - g_{1,j}^{theor})^2}{(\Delta g_{1,j}^{data})^2} \right] , \quad (44)$$

where the sums run over all data sets and in each data set over all data points. The minimization of the χ^2 value above to determine the best parameterization of the polarized parton distributions is done using the program MINUIT [45]. Only fits giving a positive definite covariance matrix at the end have been accepted in order to be able to calculate the fully correlated 1σ error bands.

5 Parameterizations of the Polarized Parton Distributions and their Errors

5.1 Parameterization of the Parton Densities

The shape chosen for the parameterization of the polarized parton distributions in x -space at the input scale of $Q_0^2 = 4.0 \text{ GeV}^2$ is

$$x\Delta f_i(x, Q_0^2) = \eta_i A_i x^{a_i} (1-x)^{b_i} \left(1 + \gamma_i x + \rho_i x^{\frac{1}{2}} \right) . \quad (45)$$

The term x^{a_i} controls the low- x behavior of the parton densities and $(1-x)^{b_i}$ that at large values of x . The remainder polynomial factor accounts for the additional medium- x degrees of freedom. The normalization constants A_i

$$A_i^{-1} = \left(1 + \gamma_i \frac{a_i}{a_i + b_i + 1} \right) B(a_i, b_i + 1) + \rho_i B\left(a_i + \frac{1}{2}, b_i + 1\right) \quad (46)$$

are chosen such that the η_i are the first moments of $\Delta q_i(x, Q_0^2)$, $\eta_i = \int_0^1 dx \Delta q_i(x, Q_0^2)$. Here $B(a, b)$ is the Euler Beta-function being related to the Γ -function by

$$B(a, b) = \frac{\Gamma(a)\Gamma(b)}{\Gamma(a+b)} . \quad (47)$$

In the present approach the QCD-evolution equations are solved in MELLIN- N space as described in section 2. The MELLIN-transform of the parton densities is performed and MELLIN- N moments are calculated for complex arguments N :

$$\begin{aligned} \mathbf{M}[\Delta f(x, Q_0^2)](N) &= \int_0^1 x^{N-1} \Delta f(x, Q_0^2) dx \\ &= \eta_i A_i \left(1 + \gamma_i \frac{N-1+a_i}{N+a_i+b_i} \right) B(N-1+a_i, b_i+1) \\ &\quad + \rho_i B \left(N+a_i - \frac{1}{2}, b_i+1 \right) . \end{aligned} \quad (48)$$

As seen from Eq. (45) there are five parameters for each parton distribution. To meet both the quality of the present data and the reliability of the fitting program the number of parameters has to be reduced. Assuming $SU(3)$ flavor symmetry and a flavor symmetric sea one only has to derive one general polarized sea-quark distribution. The first moments of the polarized valence distributions Δu_v and Δd_v can be fixed by the $SU(3)$ parameters F and D as measured in neutron and hyperon β -decays according to the relations :

$$\eta_{u_v} - \eta_{d_v} = F + D , \quad (49)$$

$$\eta_{u_v} + \eta_{d_v} = 3F - D . \quad (50)$$

A re-evaluation of F and D was performed in Ref. [15] on the basis of updated β -decay constants [49] leading to

$$\eta_{u_v} = 0.926 \pm 0.014 , \quad (51)$$

$$\eta_{d_v} = -0.341 \pm 0.018 . \quad (52)$$

Given the present accuracy of the data a number of parameters is set to zero, namely $\rho_{u_v} = \rho_{d_v} = 0$, $\gamma_{\bar{q}} = \rho_{\bar{q}} = 0$, and $\gamma_G = \rho_G = 0$. This choice reduces the number of parameters to be fitted for each polarized parton density to three. In addition the QCD parameter Λ_{QCD} is to be determined. We allow for a relative normalization shift between the different data sets within the normalization uncertainties quoted by the experiments. These normalization shifts were fitted once and then fixed afterwards.

The polarized parton densities to be determined are chosen to be

$$\begin{aligned} \Delta u_v(x) &= \Delta u(x) - \Delta \bar{u}(x) , \\ \Delta d_v(x) &= \Delta d(x) - \Delta \bar{d}(x) , \\ \frac{1}{6} \Delta \bar{Q}(x) &= \Delta \bar{q}(x) = \Delta \bar{u}(x) = \Delta \bar{d}(x) = \Delta s(x) = \Delta \bar{s}(x) , \\ \text{and } \Delta G(x) &. \end{aligned} \quad (53)$$

Twelve parameters representing the parton densities are determined in the fit. These are : for Δu_v : a_{u_v} , b_{u_v} , and γ_{u_v} , for Δd_v : a_{d_v} , b_{d_v} , and γ_{d_v} , for $\Delta \bar{Q}$: $\eta_{\bar{q}}$, $a_{\bar{q}}$, and $b_{\bar{q}}$, and for ΔG : η_G , a_G , and b_G . Note that $\eta_{\bar{q}}$ represents the first moment of the total quark sea. Starting off with these parameters the analysis shows, however, that the four parameters γ_{u_v} , γ_{d_v} , $b_{\bar{q}}$, and b_G turn

out to have very large errors at χ_{\min}^2 . Altering them within the error range does not lead to a significant change of χ^2 , which shows that they are badly constrained by the inclusive data used in the analysis. We, therefore, fixed these parameters at their values obtained at the end of the fit and consider them as outer model-parameters. It is not expected that the small- x behavior of the polarized gluon and the sea-quarks is much different. To achieve this it turned out that the small- x slopes of the gluon and the sea-quarks are to be related like $a_G = a_{\bar{q}} + C$, with $C = 0.5 \dots 1.0$. We therefore decided to fix one of the parameter relative to the other. In fixing the high- x slopes b_G and $b_{\bar{q}}$ we adopted a relation as derived from the unpolarized parton densities, namely $b_{\bar{q}}/b_G(\text{pol}) = b_{\bar{q}}/b_G(\text{unpol})$ (see e.g. Ref. [27]). Both relations together are suited to lead to positivity for ΔG and $\Delta \bar{q}$.¹⁰ No positivity constraint was assumed for Δu_v and Δd_v . After this the statistical measurement is only applied to the remaining seven parameters which describe the parton densities and to Λ_{QCD} .

5.2 Error Calculation

The evolved polarized parton densities and structure functions are linear functions of the input densities. Let $f(x, Q^2; a_i|_{i=1}^k)$ be the evolved density at Q^2 depending on the parameters $a_i|_{i=1}^k$. Then its correlated error as given by Gaussian error propagation is

$$\Delta f(x, Q^2) = \left[\sum_{i=1}^k \left(\frac{\partial f}{\partial a_i} \right)^2 C(a_i, a_i) + \sum_{i \neq j=1}^k \left(\frac{\partial f}{\partial a_i} \frac{\partial f}{\partial a_j} \right) C(a_i, a_j) \right]^{\frac{1}{2}}, \quad (54)$$

where $C(a_i, a_j)$ are the elements of the covariance matrix determined in the QCD analysis at the scale Q_0^2 . The gradients $\partial f / \partial a_i$ at this scale can be calculated analytically, except for Λ_{QCD} . Their value at Q^2 is calculated by evolution. The general form of the derivative of the MELLIN moment $\mathbf{M}[f(a)](N)$ w.r.t. the parameter a is

$$\frac{\partial \mathbf{M}[f(a)](N)}{\partial a} = F(a) \times \mathbf{M}[f(a)](N) \quad (55)$$

for complex values of N . Here we give the relevant expressions for $F(a)$ as the normalized gradients w.r.t. the parameters being varied in the final fit, which are finally two parameters per distribution. For the polarized parton distributions Δu_v and Δd_v one obtains

$$\begin{aligned} F(a_i) &= \psi(N - 1 + a_i) - \psi(N + a_i + b_i) \\ &\quad + \left(\frac{\gamma_i(b_i + 1)}{(N + a_i + b_i)(N + a_i + b_i + \gamma_i(N - 1 + a_i))} \right) \\ &\quad - \psi(a_i) + \psi(a_i + b_i + 1) - \left(\frac{\gamma_i(b_i + 1)}{(a_i + b_i + 1)(a_i + b_i + 1 + \gamma_i a_i)} \right), \end{aligned} \quad (56)$$

$$\begin{aligned} F(b_i) &= \psi(b_i + 1) - \psi(N + a_i + b_i) \\ &\quad - \left(\frac{\gamma_i(N - 1 + a_i)}{(N + a_i + b_i)(N + a_i + b_i + \gamma_i(N - 1 + a_i))} \right) \\ &\quad - \psi(b_i + 1) + \psi(a_i + b_i + 1) + \left(\frac{\gamma_i a_i}{(a_i + b_i + 1)(a_i + b_i + 1 + \gamma_i a_i)} \right), \end{aligned} \quad (57)$$

¹⁰For a discussion of positivity of parton densities see [50].

whereas for $\Delta\bar{q}$ and ΔG

$$F(\eta_i) = \frac{1}{\eta_i}, \quad (58)$$

$$F(a_i) = \psi(N-1+a_i) - \psi(N+a_i+b_i) - \psi(a_i) + \psi(a_i+b_i+1). \quad (59)$$

Here $\psi(z) = d/dz(\log \Gamma(z))$ denotes the EULER ψ -function. The gradients evolved in MELLIN space are then transformed back to x space and are used according to Eq. (54). To obtain the gradients for the error calculation of the polarized structure functions g_1^p and g_1^n , which are composed of the polarized parton densities the expressions above, Eqs. (56–59) have to be multiplied with the corresponding Wilson coefficient functions.

This yields the errors as far as the QCD parameter Λ_{QCD} is fixed and regarded as uncorrelated. The inclusion of the QCD parameter is performed easiest by numerical methods due to non-linear and iterative aspects in the calculation of $\alpha_s(Q^2, \Lambda_{\text{QCD}})$. The respective gradients are calculated performing the evolution both for $\Lambda \pm \delta$, with $\delta \ll \Lambda$

$$\frac{\partial f(x, Q^2, \Lambda)}{\partial \Lambda} = \frac{f(x, Q^2, \Lambda + \delta) - f(x, Q^2, \Lambda - \delta)}{2\delta} \quad (60)$$

using values for $\delta \sim 10$ MeV in the present analysis.

Finally we also present the gradients at the input scale Q_0^2 in x -space for completeness, also w.r.t. the parameters being fixed in the final analysis :

$$\frac{\partial \Delta q_i}{\partial \eta_i} = \frac{1}{\eta_i} \Delta q_i, \quad \frac{\partial \Delta q_i}{\partial a_i} = \left(\log(x) - \frac{1}{T} \frac{\partial T}{\partial a_i} \right) \Delta q_i, \quad (61)$$

$$\frac{\partial \Delta q_i}{\partial b_i} = \left(\log(1-x) - \frac{1}{T} \frac{\partial T}{\partial b_i} \right) \Delta q_i, \quad \frac{\partial \Delta q_i}{\partial \gamma_i} = \left(\frac{x}{1 + \gamma_i x + \rho_i x^{\frac{1}{2}}} - \frac{1}{T} \frac{\partial T}{\partial \gamma_i} \right) \Delta q_i, \quad (62)$$

$$\frac{\partial \Delta q_i}{\partial \rho_i} = \left(\frac{x^{\frac{1}{2}}}{1 + \gamma_i x + \rho_i x^{\frac{1}{2}}} - \frac{1}{T} \frac{\partial T}{\partial \rho_i} \right) \Delta q_i, \quad (63)$$

with

$$T = B(a_i, b_i + 1) \left(1 + \frac{\gamma_i a_i}{1 + a_i + b_i} \right) + \gamma_i B\left(a_i + \frac{1}{2}, b_i + 1\right), \quad (64)$$

$$\frac{\partial T}{\partial a_i} = [\psi(a_i) - \psi(a_i + b_i + 1)] B(a_i, b_i + 1) \left(1 + \frac{\gamma_i a_i}{1 + a_i + b_i} \right) + B(a_i, b_i + 1) \quad (65)$$

$$\times \left(\frac{\gamma_i a_i}{(1 + a_i + b_i)^2} \right) + \left[\psi\left(a_i + \frac{1}{2}\right) - \psi\left(a_i + b_i + \frac{3}{2}\right) \right] \rho_i B\left(a_i + \frac{1}{2}, b_i + 1\right), \quad (66)$$

$$\begin{aligned} \frac{\partial T}{\partial b_i} &= [\psi(b_i + 1) - \psi(a_i + b_i + 1)] B(a_i, b_i + 1) \left(1 + \frac{\gamma_i a_i}{1 + a_i + b_i} \right) - B(a_i, b_i + 1) \\ &\times \left(\frac{\gamma_i a_i}{(1 + a_i + b_i)^2} \right) + \left[\psi(b_i + 1) - \psi\left(a_i + b_i + \frac{3}{2}\right) \right] \rho_i B\left(a_i + \frac{1}{2}, b_i + 1\right), \end{aligned} \quad (67)$$

$$\frac{\partial T}{\partial \gamma_i} = B(a_i, b_i + 1) \left(\frac{a_i}{1 + a_i + b_i} \right), \quad (68)$$

$$\frac{\partial T}{\partial \rho_i} = B\left(a_i + \frac{1}{2}, b_i + 1\right). \quad (69)$$

Both approaches have been used at the input scale and delivered the same error contours.

6 Results of the QCD Analysis

6.1 Standard QCD Analysis

In the fitting procedure we started with the 13 parameters selected, i.e. three parameters for each of the four polarized parton distribution and Λ_{QCD} to be determined. For this set of parameters the sea-quark distribution was assumed to be described according to $SU(3)$ flavor symmetry. This assumption is justified for an *inclusive* data analysis, which we aim on in this paper, given the present accuracy of the data, which may be refined in the forthcoming by including also semi-inclusive data, which become more and more precise. Analyzing the constraints of the different parameters at χ^2_{min} , it turns out that the deep-inelastic scattering data do not constrain the four parameters γ_{u_v} , γ_{d_v} , $b_{\bar{q}}$, and b_G sufficiently well, since rather large errors for these quantities are obtained. In the further procedure we fixed these parameters at their values obtained in the first minimization and chose the ratio $b_{\bar{q}}/b_G$ as in the unpolarized case [46]. Let us note that the latter choice is one possible option. The lack of constraining power of the present data on the polarized parton densities has to be stressed, however. Only more precise data in this range can improve the situation in the future. In the fit we found some tendency towards a harder distribution for the gluon, although being not significant given the errors obtained for the large- x parameters. It also turns out that the small- x parameter for the gluon and the sea-quark distribution take essentially values which are shifted relative to each other as $\alpha_G = \alpha_S + c$ with $c \sim 0.5 \dots 1$, with some preference according to the value of χ^2_{min} . This lead to values of $c = 0.9, 0.6$ in LO (ISET=1,2) and $c = 0.9, 0.5$ for the NLO parameterizations (ISET = 3,4), cf. Appendix 1.

The final minimization was carried out under the above conditions and determined the remaining eight parameters with their 1σ errors and the corresponding covariance matrix elements. Only fits ending with a positive-definite covariance matrix were accepted. The values and errors of these parameters along with those parameters fixed in the parameterization, cf. section 5, are summarized for both values of c in LO and NLO in table 2 for the parameters of the non-perturbative input distributions. The results on Λ_{QCD} are discussed separately in section 6.2. The starting scale of the evolution was chosen as $Q_0^2 = 4 \text{ GeV}^2$. The covariance matrix elements for the LO and NLO fits, from which the parameterizations ISET=1...4 are derived, are given in tables 3–6.

In Figures 1–4 the fitted parton distribution functions in leading and next-to-leading order for all sets of parameterizations and their 1σ errors are presented at the starting scale Q_0^2 . The positivity bounds as e.g. obtained referring to the unpolarized distributions [46] hold either for the central value itself or well within the present error bands. The current data constrain the up-valence distribution at best, followed by the down-valence, sea-quark, and gluon distributions. Our leading order results deviate from previous parameterizations [15, 16] somewhat at lower values of x . Except for the gluon distribution this deviation is much less in next-to-leading order, taking into account the experimental 1σ errors. In the range $x \in [10^{-3}, 1]$ the polarized up-valence and gluon distributions are positive within errors, while the sea-quark and the down-valence densities are negative at the reference scale $Q_0^2 = 4 \text{ GeV}^2$, the latter except in a small range at very large x .

In Figure 5 the NLO polarized gluon densities of ISET =3,4, are compared to the unpolarized gluon distribution of Ref. [46], to which the error of the gluon density as determined by the H1 experiment [47] is overlaid symmetrically in the range $x > 0.1$. Both error contours illustrate the current margin of the positivity constraint for the gluon density, which is well covered.

The polarized structure function $xg_1^p(x, Q^2)$ measured in the interval $3.0 \text{ GeV}^2 < Q^2 <$

5.0 GeV², Figure 6, using the world asymmetry data is well described by our QCD NLO curve and the 1 σ error band. We also compare to corresponding representations of the parameterizations [15, 16], which are compatible within the present errors.

Looking at the Q^2 dependence of the structure function $g_1(x, Q^2)$ in intervals of x gives insight to the scaling violations in the spin sector. As in the unpolarized case the presence of scaling violations are expected to manifest in a slope changing with x . The world proton data on $g_1(x, Q^2)$ have been plotted in such a way in Figure 7 and confronted with the QCD NLO curves of the present analysis and its 1 σ error bands. Corresponding curves of the parameterizations [15, 16] are also shown. Slight but non-significant differences between the different analyzes are observed in the intervals at low values of x . However, the data are well covered within the errors by all three analyzes. The current statistics in the low- x range is still rather low.

In Figures 8–11 the scaling violations of the individual polarized momentum densities are depicted in the range $x \in [10^{-3}, 1]$, $Q^2 \in [1, 10^4]$ GeV² choosing the NLO distributions of ISET=3 as an example. The up-valence distribution $x\Delta u_v$, Figure 8, evolves towards smaller values of x and the peak around $x \sim 0.25$ becomes more flat in the evolution from $Q^2 = 1$ GeV² to $Q^2 = 10^4$ GeV². The distribution is positive within the errors. Statistically this distribution is constrained best among all others. The down-valence distribution $x\Delta d_v$, Figure 9, remains negative in the same range, although it is less constraint by the present data than the up-valence density. Also here the evolution is towards smaller values of x and structures at larger x flatten out. The momentum density of the polarized gluon $x\Delta G$, Figure 10, is positive in the depicted range for $Q^2 \geq 4$ GeV², but becomes slightly negative for smaller values of x at $Q^2 \sim 1$ GeV². Also in this case the evolution moves the shape towards lower values of x and flattens the distribution. The error band becomes more uniformly. The sea-quark distribution $x\Delta \bar{q}$, Figure 11, is negative in the kinematic range shown for $Q^2 \leq 10$ GeV² and remains negative within errors for $x \leq 5 \cdot 10^{-2}$ up to $Q^2 = 10^4$ GeV², but changes sign for larger values of x . The minimum of the distribution at $Q^2 = 1$ GeV² around $x \sim 0.1$ moves to $x \sim 0.01$ at $Q^2 = 10^4$ GeV². At the same time a maximum at $x \sim 0.1$ occurs.

In the present analysis the structure functions $g_1^{p,n}(x, Q^2)$ were parameterized in the twist-2 approximation at next-to-leading order. As the data may contain higher twist terms as well it is of interest to look for the potential effect of these contributions. At present the size of twist-4 contributions in deep-inelastic scattering data is widely unknown both in the unpolarized and polarized case¹¹. Due to this we use the following phenomenological ansätze for a higher twist term :

$$h_I(x, Q^2) = 1 + \frac{A}{Q^2} x^\alpha (1-x)^\beta, \quad (70)$$

$$h_{II}(x, Q^2) = 1 + \frac{1}{Q^2} [A + Bx + Cx^2], \quad (71)$$

which are used multiplicatively with $g_1(x, Q^2)$. We compare these fit results with the NLO parameterization ISET = 4 in Figure 12. Both ansätze yield results of similar size and deviate from the NLO curves at small values of Q^2 , however, they are fully consistent with the NLO results within the 1 σ error (hatched area). This shows that the present data do not contain significant higher twist contributions in the range $Q^2 > 1$ GeV² and a NLO analysis can be carried out. This is also reflected by the observed logarithmic scaling violations, Figures 7, 12, and the measurement of the QCD scale Λ_{QCD} , to which we turn now.

¹¹For a recent analysis of gluon induced contributions in the unpolarized case see Ref. [54].

6.2 Λ_{QCD} and $\alpha_s(M_Z)$

In the QCD analysis we parameterized the strong coupling constant α_s in terms of four massless flavors determining $\Lambda_{QCD}^{(4)\overline{MS}}$. The NLO result fitting the asymmetry data, g_1/F_1 or A_1 , is

$$\Lambda_{QCD}^{(4)\overline{MS}} = 235 \pm 53 \text{ (stat) MeV, ISET} = 3, \quad (72)$$

$$\Lambda_{QCD}^{(4)\overline{MS}} = 240 \pm 60 \text{ (stat) MeV, ISET} = 4, \quad (73)$$

identifying both the factorization and renormalization scales with Q^2 . The stability of the NLO result was investigated by changing both scales to values different of Q^2 . Since the present range in Q^2 probed in polarized deep inelastic scattering is still rather low we vary Q^2 only by factors of 2 and keep the other scale at Q^2 . The following variations are obtained:

$$\Delta\Lambda_{QCD}^{(4)\overline{MS}} = \begin{matrix} +61 \\ -47 \end{matrix} \text{ (fac)} \begin{matrix} -61 \\ +114 \end{matrix} \text{ (ren) MeV, ISET} = 3 ,$$

$$\Delta\Lambda_{QCD}^{(4)\overline{MS}} = \begin{matrix} +58 \\ -45 \end{matrix} \text{ (fac)} \begin{matrix} -66 \\ +123 \end{matrix} \text{ (ren) MeV, ISET} = 4 .$$

These results can be expressed in terms of $\alpha_s(M_Z^2)$:

$$\alpha_s(M_Z^2) = 0.113 \begin{matrix} +0.004 \\ -0.004 \end{matrix} \text{ (stat)} \begin{matrix} +0.004 \\ -0.004 \end{matrix} \text{ (fac)} \begin{matrix} +0.008 \\ -0.005 \end{matrix} \text{ (ren) , ISET} = 3,$$

$$\alpha_s(M_Z^2) = 0.114 \begin{matrix} +0.004 \\ -0.005 \end{matrix} \text{ (stat)} \begin{matrix} +0.004 \\ -0.004 \end{matrix} \text{ (fac)} \begin{matrix} +0.008 \\ -0.006 \end{matrix} \text{ (ren), ISET} = 4 .$$

Combining the errors these values

$$\alpha_s(M_Z^2) = 0.113 \begin{matrix} +0.010 \\ -0.008 \end{matrix} , \quad (74)$$

$$\alpha_s(M_Z^2) = 0.114 \begin{matrix} +0.010 \\ -0.009 \end{matrix} , \quad (75)$$

can be compared with results from other QCD analyzes of polarized inclusive deep-inelastic scattering data

$$\begin{aligned} \text{E154 [51]} : \quad \alpha_s(M_Z^2) &= 0.108 - 0.116, \quad \text{bad for } \geq 0.120 , \\ \text{SMC [52]} : \quad \alpha_s(M_Z^2) &= 0.121 \pm 0.002(\text{stat}) \pm 0.006(\text{syst} + \text{theor}) , \\ \text{ABFR [14]} : \quad \alpha_s(M_Z^2) &= 0.120 \begin{matrix} +0.004 \\ -0.005 \end{matrix} \text{ (exp)} \begin{matrix} +0.009 \\ -0.006 \end{matrix} \text{ (theor)} , \end{aligned} \quad (76)$$

and with the value of the current world average

$$\alpha_s(M_Z^2) = 0.118 \pm 0.002 \text{ [53]} . \quad (77)$$

The results of the present analysis are consistent within 1σ although our result and that of E154 [51] lead to a somewhat lower central value for $\alpha_s(M_Z^2)$. In the scheme-invariant analysis, which allows for an alternative view, a minor shift for $\Lambda_{QCD}^{(4)\overline{MS}}$ down by 12 MeV was found leading

to a central value of $\alpha_s(M_Z^2) = 0.113$ with statistical and the renormalization scale dependent errors of the same size as quoted above. Still more systematic effects have to be investigated in the future. Here we see a main point in studying further the unpolarized structure function $F_1(x, Q^2)$, the denominator function in the expression for the spin asymmetry. In our analysis it was obtained from parameterizations of F_2 [44] and R [34] measurements which themselves are subject to systematic uncertainties.

6.3 Scheme-Invariant Analysis

A factorization–scheme invariant QCD analysis in next–to–leading order based on the observables $g_1(x, Q^2)$ and $\partial g_1(x, Q^2)/\partial t$ for the proton has been performed, where t is the evolution variable defined in Eq. (24), see section 3. If compared to the standard analysis these two observables take the roles of $\Delta\Sigma(x, Q^2)$ and $\Delta G(x, Q^2)$. Such an analysis has, in principle, the advantage of direct experimental control over the input densities since they are *measurable* quantities. In this way no ansatz for ΔG is necessary and the only free parameter to be determined is Λ_{QCD} . Unfortunately, the quality of the present data does not yet allow an experimental determination of the slope $\partial g_1(x, Q^2)/\partial t$ accurate enough to be used as input density. In the present analysis this slope has been derived fitting the world data as described in section 3. In the singlet analysis the initial distributions are $g_1^S(x, Q_0^2)$ and $\partial g_1^S(x, Q_0^2)/\partial t$. The latter quantity is depicted in Figure 13 as a function of x together with the corresponding slopes at higher values of Q^2 . This slope has a rather involved shape and it requires precise data in the range of the input scale Q_0^2 on $g_1(x, Q^2)$ to determine the slope experimentally in the future. The QCD analysis performed lead to a downward shift of 12 MeV for Λ_{QCD} which yields a similar result for $\alpha_s(M_Z^2)$ as obtained in the standard analysis, see section 6.2.

7 Moments of Polarized Parton Distributions

In recent lattice simulations [23–25] low moments for the polarized parton densities $\Delta u_v, \Delta d_v$, and $\Delta u - \Delta d$ were determined. These moments are

$$\langle x^{n+1} \rangle_{\Delta f} = \int_0^1 x^{n+1} \left[\Delta f(x) + (-1)^{(n+1)} \Delta \bar{f}(x) \right] dx = \mathbf{M}[\Delta f(x)](n) + (-1)^{(n+1)} \mathbf{M}[\Delta \bar{f}(x)](n) , \quad (78)$$

for $n = -1, 0, 1$. The results of the simulation are presented at a scale $\mu^2 = 1/a^2 \sim 4 \text{ GeV}^2$, where a denotes the lattice spacing. The values of these lattice moments may be compared with the moments being obtained in the present analysis. Moreover we also present the respective moments for the sea–quark and gluon distributions and include their 1σ error. Moments of structure functions or parton distributions based on a data analysis are only constrained in the range of the respective measurements. No definite statement can be made on the behavior of the (non-perturbative) parton distributions outside the range being explored.¹² Reliably precise estimates neither for the range of very low [20] nor large x are available currently. Due to this the value and error of the moments given below is that derived from the current experimental constraints. Nonetheless we study which contribution of the moments is determined by the range in which measurements exist.

¹²Note that before 1992 the strong growth of the structure function $F_2(x, Q^2)$, later found even at very low scales $Q^2 \sim 2 \text{ GeV}^2$, came as a surprise [55]. Likewise, at present the unpolarized gluon and sea–quark distributions at large values of x are widely unknown.

In Table 7 the moments of the NLO parton densities and some of their combinations, being derived in the present analysis, and their 1σ errors are given. We also compare to the respective values obtained integrating only over the kinematic range in which data are measured and quote the value below and above the kinematic range for the moments of the NLO parton densities ISET=3,4. The determination of the error of the moments requires in general a correlated error propagation through the evolution equations, if the reference scale Q^2 is not the input scale Q_0^2 . As the lattice calculations provide measurements for a series of moments at the starting scale chosen in the present analysis the formulae given in section 5.2. apply directly. Whereas the estimated uncertainty for the distributions ISET = 3,4 for the unmeasured large- x range $x > 0.85$ is small, it is quite significant for the lowest moment for the small- x range, $x < 0.02$. For the up-quark distributions and their combinations the present correlated 1σ errors are about 10% for the lowest moments, and reach about 30% for the down quark, and 25% for the sea quarks. Depending on the parameterization the lowest moment of the polarized gluon distribution is found to have an error of 50% and more. Towards higher moments the errors grow, but the small- x uncertainties become less significant. The first three moments of the distributions $\Delta u_v(x)$, $\Delta d_v(x)$ and $\Delta u(x) - \Delta d(x)$ can be compared with lattice results [23–25], with some caution. Only for a part of these values continuum extrapolations were yet performed. Still further study is required to safely determine and quantify systematic errors. While for the distribution $\Delta u - \Delta d$ the moment for $n = -1$ comes out to be too small in the lattice measurements, it is somewhat too large for the moments $n = 0, 1$. We quote for the lowest moment an error, which is obtained due to all correlated parameters in the fit. On the other hand, the central value given is the axial charge g_A , which is much more precisely determined by other measurements. It is yet difficult to see a systematic trend in the lattice values comparing to the moments found in the present analysis. Given the fact, that higher moments are more difficult to measure the agreement of the first two moments within the errors determined in the present analysis is quite good.

We also compare the first moments in NLO with other recent analyzes, see table 8. Although some of the numbers, particularly for the gluon and sea-quark distributions look different they agree perfectly within the 1σ errors derived in our analysis.

8 Conclusions

We have performed a QCD analysis of the inclusive polarized deep-inelastic charged lepton-nucleon scattering world data to next-to-leading order and derived parameterizations of polarized parton distributions at a starting scale Q_0^2 together with the QCD-scale Λ_{QCD} . The analysis was performed using the χ^2 -method to determine the parameters of the problem in a fit to the data. A new aspect in comparison with previous analyzes is that we determine also the fully correlated errors of the parton densities and the QCD scale in leading and next-to-leading order. Due to the fact that not all shape parameters of the parton densities can be measured at sufficient accuracy using the present data, we derived two sets of parameterizations, which mainly differ in the low- x behavior of the gluon densities. Detailed comparisons were performed to the results obtained in other recent parameterizations [15, 16]. The previous results are widely compatible with the present parameterizations within the current 1σ error bands. Since we used the MELLIN-method to solve the evolution equations the Gaussian error propagation of the parameters of the input densities through the evolution was possible in analytic form. Both the central values and the 1σ errors of the parton densities are made available in form of a numerical pa-

parameterizations in the kinematic range $x \in [10^{-9}, 1]$, $Q^2 \in [1, 10^6]$ GeV². These distributions can be used in the numerical calculations for polarized high-energy scattering processes at hadron- and ep -colliders. Moreover, due to the fact that parameterizations of the errors are available, error estimates of these quantities are possible w.r.t. the present knowledge of parton densities. These parameterizations are available as fast FORTRAN-routines which makes their application possible in Monte Carlo simulations.

The current experimental data allow to measure the QCD scale Λ_{QCD} with a statistical error of $\delta\Lambda = \pm 60$ MeV, and $\delta\alpha_s(M_Z^2) \pm 0.004$. Since at present only a next-to-leading order analysis can be carried out the variations in the renormalization and factorization scales induce yet large systematic errors. Combining all errors one obtains for the two scenarios (ISET = 3, 4) $\alpha_s(M_Z^2) = 0.113 \pm \begin{smallmatrix} 0.010 \\ 0.008 \end{smallmatrix}$ and $\alpha_s(M_Z^2) = 0.114 \pm \begin{smallmatrix} 0.010 \\ 0.009 \end{smallmatrix}$, respectively. The theoretical error due to the present renormalization and factorization scale uncertainties can be further reduced in a three-loop analysis, for which the anomalous dimensions have still to be calculated. We also performed for the first time a factorization scheme-invariant QCD analysis based on $g_1(x, Q^2)$ and $\partial g_1(x, Q^2)/\partial \log Q^2$ which lead to a small shift of 12 MeV in Λ_{QCD} only. This novel way of analysis which is based on the scaling violations of *observables* directly may show its full strengths in later analyzes based on the even higher statistics of future experiments. In this analysis factorization scale uncertainties do not occur.

The results of the present analysis may be compared to recent lattice results calculating the first few moments of the distributions $\Delta u_v(x, Q^2)$, $\Delta d_v(x, Q^2)$, and $\Delta(u_v - d_v)(x, Q^2)$ and their respective errors. We also present the respective moments of $\Delta \bar{q}(x, Q^2)$ and $\Delta G(x, Q^2)$ for which lattice results do not exist at present. Both on the side of the lattice measurements and the extraction of the distribution functions from deep inelastic scattering data the errors improved during recent years and the values became closer. However, more work has yet to be done in the future on systematic effects and even more precise experimental data would be welcome to perform an essential test of QCD also in this field at a higher precision than possible at present.

Acknowledgment. This work was supported in part by EU contract FMRX-CT98-0194 (DG 12 - MIHT). For discussions in an early phase of this work we would like to thank Andreas Vogt. For discussions we thank W.-D. Nowak. We thank Stefano Forte and Giovanni Ridolfi for recalculating the first moments from their previous analyzes in the $\overline{\text{MS}}$ scheme. For discussion on recent lattice results we thank S. Capitani, K. Jansen, and G. Schierholz.

9 Appendix: The FORTRAN-code for the parton densities and their errors

A fast FORTRAN program is available to represent the polarized parton densities $x\Delta u_v(x, Q^2)$, $x\Delta d_v(x, Q^2)$, $x\Delta G(x, Q^2)$, and $x\Delta\bar{q}(x, Q^2)$ and the polarized structure functions $xg_1^p(x, Q^2)$ and $xg_1^n(x, Q^2)$ in leading and next-to-leading order in the $\overline{\text{MS}}$ -scheme together with the parameterizations of their 1σ errors. The following ranges in x and Q^2 are covered:

$$10^{-9} < x < 1 \quad , \quad 1 \text{ GeV}^2 < Q^2 < 10^6 \text{ GeV}^2.$$

The polarized distributions are the result of a fit to the world data on spin asymmetries, i.e. $A_1^{p,n,d}$ or $g_1/F_1^{p,n,d}$, as described in the paper. The SUBROUTINE PPDF returns the values of the polarized distributions, always multiplied with x , at a given point in x and Q^2 by interpolating the data on specified grids. The interpolation in x is done by cubic splines and in Q^2 by a linear interpolation in $\log(Q^2)$.¹³

The parton distributions are evaluated by

```
SUBROUTINE PPDF(ISET, X, Q2, UV, DUV, DV, DDV, GL, DGL, SEA, DSEA,
                G1P,DG1P,G1N,DG1N)
```

All non-integer variables are of the type REAL*8. The calling routine has to contain the COMMON/INTINI/ IINI. Before the first call to SUBROUTINE PPDF the initialization is set by IINI = 0. The values of the parameter ISET are:

$$\begin{aligned} \text{ISET} = 1 & \quad \text{LO,} \quad \alpha_G = \alpha_S + 0.9 \\ \text{ISET} = 2 & \quad \text{LO,} \quad \alpha_G = \alpha_S + 0.6 \\ \text{ISET} = 3 & \quad \text{NLO,} \quad \alpha_G = \alpha_S + 1.0 \\ \text{ISET} = 4 & \quad \text{NLO,} \quad \alpha_G = \alpha_S + 0.5 \end{aligned}$$

The parameters $X, Q^2/\text{GeV}^2$ are x and Q^2 . The momentum densities of the polarized up- and down valence quarks, gluons and the sea quarks are UV, DV, GL, SEA, with $\text{SEA} = x\Delta u_s = x\Delta d_s = x\Delta\bar{u} = x\Delta\bar{d} = x\Delta s = x\Delta\bar{s}$. Correspondingly, DUV is the 1σ error of UV etc. and G1P and G1N are the values of the electromagnetic structure functions g_1^p and g_1^n .

The program can be received on request via e-mail to Johannes.Bluemlein@desy.de or Helmut.Boettcher@desy.de or from <http://www-zeuthen.desy.de/~hboett/ppdf.uu.gz>.

¹³We thank S. Kumano and M. Miyama of the AAC-collaboration for allowing us to use their interpolation routines.

10 Tables

Experiment	x -range	Q^2 -range [GeV ²]	number of data points		Ref.
			g_1/F_1 or A_1	g_1	
E143(p)	0.027 – 0.749	1.17 – 9.52	82	28	[9]
HERMES(p)	0.028 – 0.660	1.13 – 7.46	39	39	[10]
E155(p)	0.015 – 0.750	1.22 – 34.72	24	24	[12]
SMC(p)	0.005 – 0.480	1.30 – 58.0	59	12	[8]
EMC(p)	0.015 – 0.466	3.50 – 29.5	10	10	[4]
proton			214	113	
E143(d)	0.027 – 0.749	1.17 – 9.52	82	28	[9]
E155(d)	0.015 – 0.750	1.22 – 34.79	24	24	[11]
SMC(d)	0.005 – 0.479	1.30 – 54.8	65	12	[8]
deuteron			171	64	
E142(n)	0.035 – 0.466	1.10 – 5.50	30	8	[5]
HERMES(n)	0.033 – 0.464	1.22 – 5.25	9	9	[6]
E154(n)	0.017 – 0.564	1.20 – 15.0	11	17	[7]/[51]
neutron			50	34	
total			435	211	

Table 1: Published data points above $Q^2 = 1.0$ GeV².

	Scenario 1				Scenario 2			
	LO		NLO		LO		NLO	
	ISET=1		ISET=3		ISET=2		ISET=4	
	value	error	value	error	value	error	value	error
$\Lambda_{QCD}^{(4)}$, MeV	203	120	235	53	195	143	240	60
η_{uv}	0.926	fixed	0.926	fixed	0.926	fixed	0.926	fixed
a_{uv}	0.197	0.013	0.294	0.035	0.199	0.013	0.271	0.029
b_{uv}	2.403	0.107	3.167	0.212	2.416	0.107	3.070	0.175
$\gamma_{uv}(*)$	21.34	fixed	27.22	fixed	21.34	fixed	27.22	fixed
η_{dv}	-0.341	fixed	-0.341	fixed	-0.341	fixed	-0.341	fixed
a_{dv}	0.190	0.049	0.254	0.111	0.182	0.046	0.325	0.125
b_{dv}	3.240	0.884	3.420	1.332	3.209	0.895	3.925	1.129
$\gamma_{dv}(*)$	30.80	fixed	19.06	fixed	30.80	fixed	19.06	fixed
η_{sea}	-0.353	0.054	-0.447	0.082	-0.314	0.053	-0.435	0.061
a_{sea}	0.367	0.048	0.424	0.062	0.428	0.055	0.285	0.048
$b_{sea}(*)$	8.51	fixed	8.93	fixed	8.51	fixed	8.93	fixed
η_G	1.281	0.816	1.026	0.554	1.043	0.938	0.931	0.679
a_G	$a_{sea} + 0.9$		$a_{sea} + 1.0$		$a_{sea} + 0.6$		$a_{sea} + 0.5$	
$b_G(*)$	5.91	fixed	5.51	fixed	5.91	fixed	5.51	fixed
χ^2 / NDF	1.02		0.90		1.04		0.93	

Table 2: Parameter values in LO and NLO (\overline{MS}) of the 7 + 1 parameter fit based on the world asymmetry data for both scenarios. The (*) marks those parameters which were fixed after the first minimization since the present data do not constrain these parameters well enough (see text).

LO								
	$\Lambda_{QCD}^{(4)}$	a_{uv}	b_{uv}	a_{dv}	b_{dv}	η_{sea}	a_{sea}	η_G
$\Lambda_{QCD}^{(4)}$	1.43E-2							
a_{uv}	-2.05E-5	1.80E-4						
b_{uv}	-9.07E-5	3.91E-4	1.15E-2					
a_{dv}	1.10E-4	1.03E-5	-2.40E-3	2.43E-3				
b_{dv}	-4.65E-5	-7.92E-3	-6.86E-3	5.48E-3	7.82E-01			
η_{sea}	1.02E-4	-4.46E-4	-2.84E-3	9.85E-4	2.82E-2	2.94E-3		
a_{sea}	-4.31E-5	1.58E-4	1.33E-3	-5.96E-4	-9.32E-3	-2.58E-4	2.29E-3	
η_G	-1.03E-3	2.02E-3	1.58E-2	-2.78E-3	-1.61E-1	-1.59E-2	9.56E-3	6.65E-1

Table 3: The covariance matrix for the 7 + 1 parameter LO fit (scenario 1, ISET = 1) based on the world asymmetry data.

NLO								
	$\Lambda_{QCD}^{(4)}$	a_{uv}	b_{uv}	a_{dv}	b_{dv}	η_{sea}	a_{sea}	η_G
$\Lambda_{QCD}^{(4)}$	2.81E-3							
a_{uv}	2.71E-5	1.22E-3						
b_{uv}	-1.30E-4	5.10E-3	4.50E-2					
a_{dv}	-3.35E-4	-5.17E-4	-3.23E-3	1.23E-2				
b_{dv}	-6.22E-4	-1.27E-2	4.65E-2	8.29E-2	1.78E-0			
η_{sea}	-5.30E-5	-2.13E-3	-1.12E-2	5.19E-3	4.74E-2	6.77E-3		
a_{sea}	-4.85E-6	9.07E-4	4.49E-3	-3.78E-3	-2.98E-2	-2.39E-3	3.82E-3	
η_G	4.03E-4	1.41E-2	6.71E-2	-3.07E-2	-2.22E-1	-3.78E-2	1.90E-2	3.07E-1

Table 4: The covariance matrix for the 7 + 1 parameter NLO fit (scenario 1, ISET = 3) based on the world asymmetry data.

LO								
	$\Lambda_{QCD}^{(4)}$	a_{uv}	b_{uv}	a_{dv}	b_{dv}	η_{sea}	a_{sea}	η_G
$\Lambda_{QCD}^{(4)}$	2.05E-2							
a_{uv}	1.25E-4	1.76E-4						
b_{uv}	-1.37E-3	3.42E-4	1.15E-2					
a_{dv}	-5.57E-4	1.89E-6	-2.19E-3	2.14E-3				
b_{dv}	9.62E-3	-7.84E-3	-1.29E-3	4.74E-3	8.00E-01			
η_{sea}	4.37E-4	-4.34E-4	-2.88E-3	1.01E-3	2.73E-2	2.86E-3		
a_{sea}	-5.78E-4	6.91E-5	4.56E-4	-3.73E-4	-2.16E-3	3.98E-4	3.06E-3	
η_G	9.43E-4	1.91E-3	1.54E-2	-1.85E-3	-1.55E-1	-1.38E-2	2.97E-3	8.80E-1

Table 5: The covariance matrix for the 7 + 1 parameter LO fit (scenario 2, ISET = 2) based on the world asymmetry data.

NLO								
	$\Lambda_{QCD}^{(4)}$	a_{uv}	b_{uv}	a_{dv}	b_{dv}	η_{sea}	a_{sea}	η_G
$\Lambda_{QCD}^{(4)}$	3.55E-3							
a_{uv}	3.09E-4	8.50E-4						
b_{uv}	1.08E-3	3.88E-3	3.06E-2					
a_{dv}	1.88E-3	2.66E-4	-8.80E-4	1.56E-2				
b_{dv}	1.74E-2	-7.57E-3	-1.34E-2	9.03E-2	1.27E-0			
η_{sea}	5.77E-4	-9.03E-4	-5.32E-3	3.26E-3	3.84E-2	3.74E-3		
a_{sea}	-5.33E-4	6.81E-4	3.68E-3	-2.28E-3	-2.56E-2	-9.06E-4	2.34E-3	
η_G	-8.19E-3	1.17E-2	5.61E-2	-3.95E-2	-3.74E-1	-2.37E-2	1.51E-2	4.61E-1

Table 6: The covariance matrix for the 7 + 1 parameter NLO fit (scenario 2, ISET=4) based on the world asymmetry data.

	n	ISET=3		ISET=4		lattice results	
		value	value out of range	value	value out of range	QCDSF	LHPC/ SESAM
Δu_v	-1	0.926 ± 0.071	0.191 4E-4	0.926 ± 0.062	0.207 4E-4	0.889(29)	0.860(69)
	0	0.163 ± 0.014	0.001 3E-4	0.160 ± 0.011	0.001 4E-4	0.198(8)	0.242(22)
	1	0.055 ± 0.006	1E-5 3E-4	0.055 ± 0.005	1E-5 3E-4	0.041(9)	0.116(42)
	2	0.024 ± 0.003	0 3E-4	0.024 ± 0.003	0 3E-4		
Δd_v	-1	-0.341 ± 0.123	-0.104 -7E-5	-0.341 ± 0.103	-0.086 -3E-5	-0.236(27)	-0.171(43)
	0	-0.047 ± 0.021	-5E-4 -6E-5	-0.049 ± 0.017	-5E-4 -3E-5	-0.048(3)	-0.029(13)
	1	-0.015 ± 0.009	-1E-5 -5E-5	-0.015 ± 0.007	-1E-5 -2E-5	-0.028(2)	0.001(25)
	2	-0.006 ± 0.005	0 -5E-5	-0.006 ± 0.004	0 -2E-5		
$\Delta u - \Delta d$	-1	1.267 ± 0.142	0.295 5E-4	1.267 ± 0.121	0.293 5E-4	1.14(3)	1.031(81)
	0	0.210 ± 0.025	0.001 4E-4	0.209 ± 0.021	0.001 4E-4	0.246(9)	0.271(25)
	1	0.070 ± 0.011	2E-5 4E-4	0.069 ± 0.009	2E-5 4E-4	0.069(9)	0.115(49)
	2	0.030 ± 0.006	0 3E-4	0.030 ± 0.004	0 3E-4		
Δu	-1	0.851 ± 0.075	0.152 4E-4	0.854 ± 0.066	0.158 4E-4		
	0	0.160 ± 0.014	8E-4 3E-4	0.158 ± 0.012	8E-4 4E-4		
	1	0.055 ± 0.006	1E-5 3E-4	0.055 ± 0.005	1E-5 3E-4		
	2	0.024 ± 0.003	0 3E-4	0.024 ± 0.003	0 3E-4		
Δd	-1	-0.415 ± 0.124	-0.144 -7E-5	-0.413 ± 0.104	-0.135 -3E-5		
	0	-0.050 ± 0.022	-7E-4 -6E-5	-0.051 ± 0.017	-7E-4 -3E-5		
	1	-0.015 ± 0.009	-1E-5 -5E-5	-0.015 ± 0.007	-1E-5 -2E-5		
	2	-0.006 ± 0.005	0 -5E-5	-0.006 ± 0.004	0 -2E-5		
$\Delta \bar{q}$	-1	-0.074 ± 0.017	-0.04 0	-0.072 ± 0.015	-0.048 0		
	0	-0.003 ± 0.001	-2E-4 0	$-0.002 \pm 5E-4$	-2E-4 0		
	1	$-4E-4 \pm 1E-4$	0 0	$-2E-4 \pm 6E-5$	0 0		
	2	$-8E-5 \pm 2E-5$	0 0	$-4E-5 \pm 1E-5$	0 0		
ΔG	-1	1.026 ± 0.549	0.04 1E-5	0.931 ± 0.669	0.191 0		
	0	0.184 ± 0.103	5E-4 1E-5	0.100 ± 0.075	0.002 0		
	1	0.050 ± 0.028	1E-5 1E-5	0.022 ± 0.017	2E-5 0		
	2	0.017 ± 0.010	0 1E-5	0.006 ± 0.005	0 0		

Table 7: Moments of the NLO parton densities and their combinations for the parameterizations ISET=3,4 at $Q^2 = 4 \text{ GeV}^2$. The value of the respective moment integrating only outside the x -range in which currently deep-inelastic scattering data are measured, $0.02 < x < 0.85$, are given for comparison (lower|upper part). The errors are the 1σ correlated errors derived in the present analysis from the polarization asymmetry world data. The values of corresponding lattice measurements, cf. [26], are shown for comparison. For $n = 0, 1$ for the values of the QCDSF collaboration no continuum extrapolation was performed.

Distribution	ISet=3	ISet=4	ABFR [14]	GRSV [16]	AAC [15]
Δu_v	0.926 ± 0.071	0.926 ± 0.062		0.9206	0.9278
Δd_v	-0.341 ± 0.123	-0.341 ± 0.103		-0.3409	-0.3416
Δu	0.851 ± 0.075	0.854 ± 0.066	$\eta_u = 0.692$	0.8593	0.8399
Δd	-0.415 ± 0.124	-0.413 ± 0.104	$\eta_d = -0.418$	-0.4043	-0.4295
$\Delta \bar{q}$	-0.074 ± 0.017	-0.072 ± 0.015		-0.0625	-0.0879
ΔG	1.026 ± 0.549	0.931 ± 0.669	1.262	0.6828	0.8076

Table 8: Comparison of the first moments of the polarized parton densities in NLO in the $\overline{\text{MS}}$ scheme at $Q^2 = 4 \text{ GeV}^2$ for different sets of recent parton parameterizations. For the ABFR-analysis [14] the values $\eta_{u,d}$ are the first moments of $\Delta u + \Delta \bar{u}$ and $\Delta d + \Delta \bar{d}$, respectively, and $\Delta s + \Delta \bar{s} = -0.081$.

11 Figures

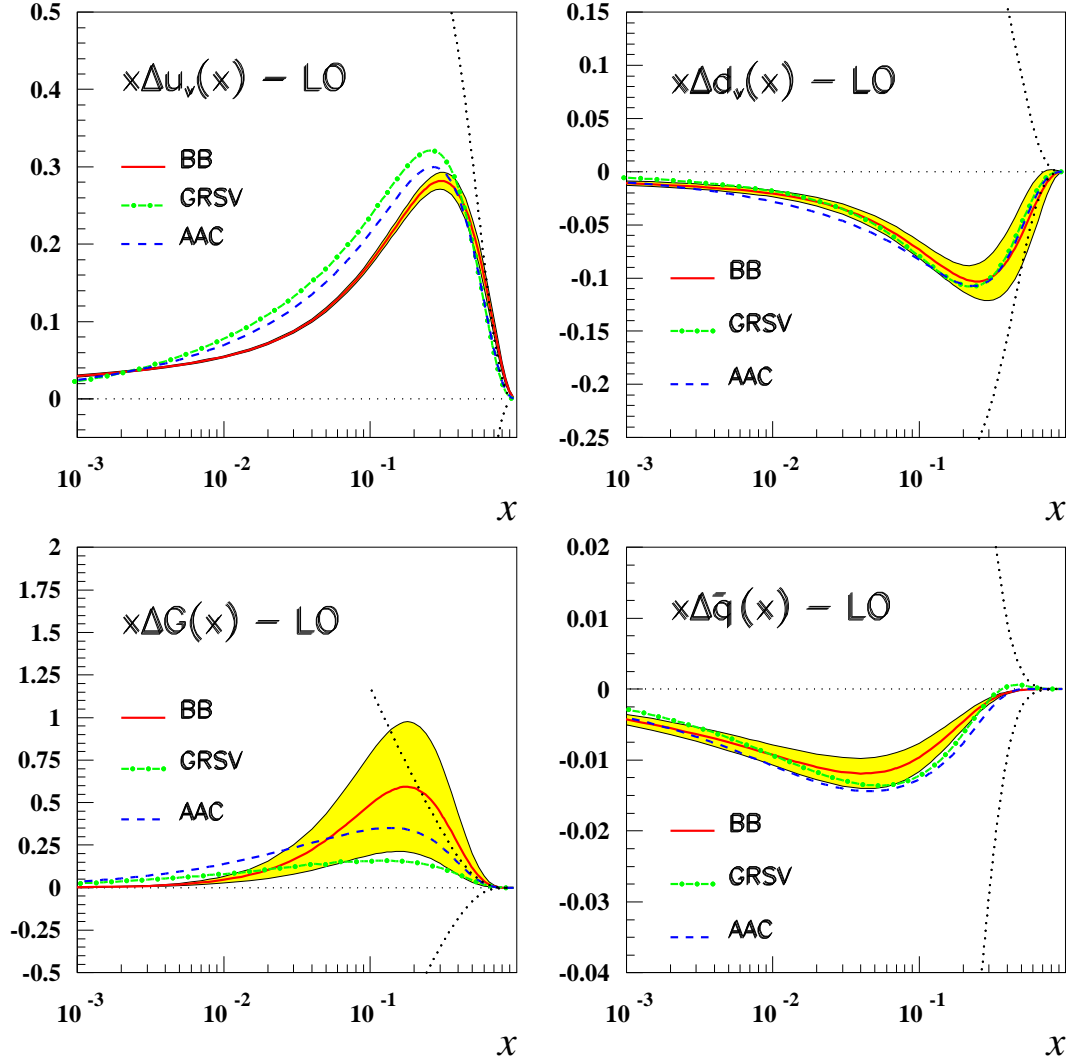


Figure 1: LO polarized parton distributions at the input scale $Q_0^2 = 4.0 \text{ GeV}^2$, $\text{ISET} = 1$, (solid line) compared to results obtained by GRSV (dashed-dotted line) [16] and AAC (dashed line) [15]. The shaded areas represent the fully correlated 1σ error bands calculated by Gaussian error propagation. The dark dotted lines indicate the positivity bounds choosing the distributions [27] for reference.

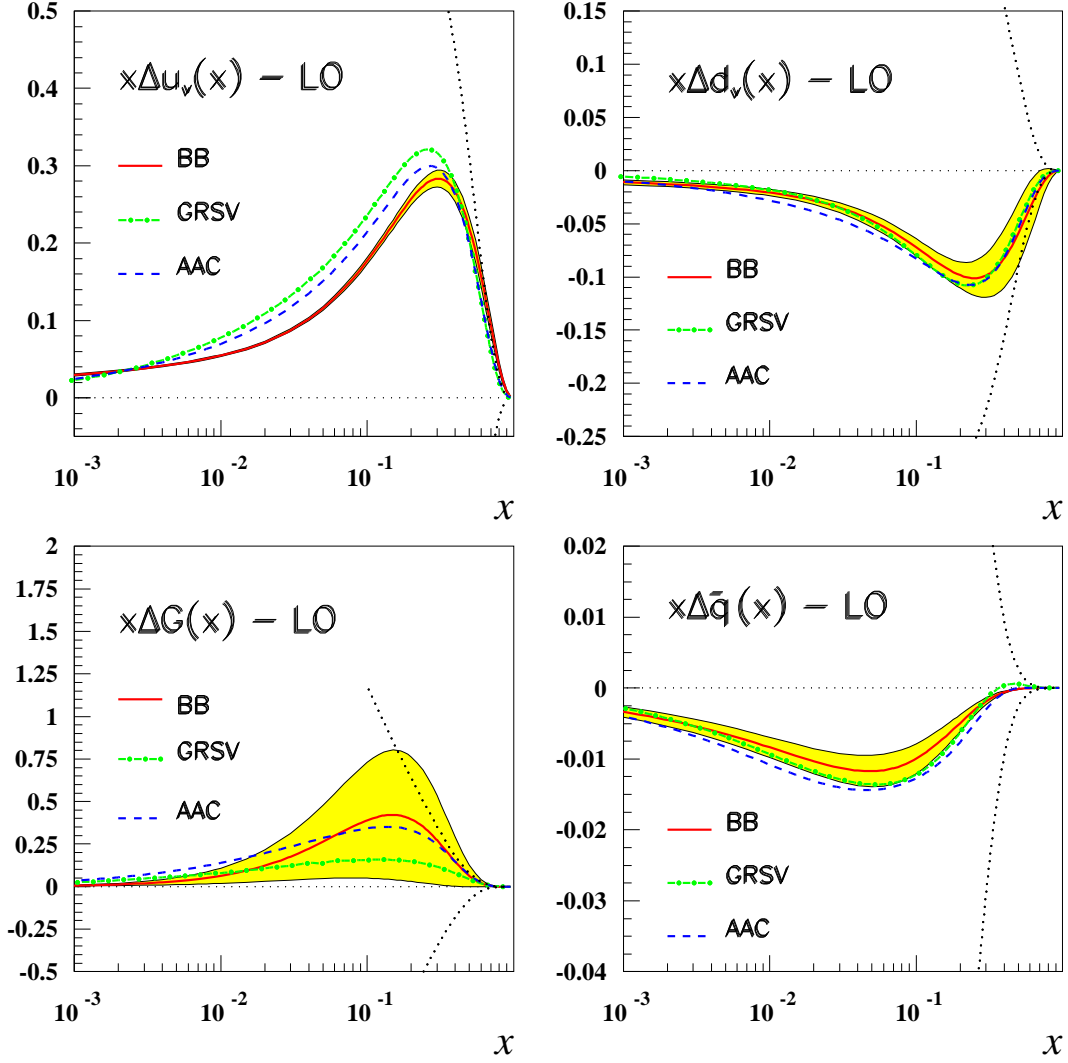


Figure 2: LO polarized parton distributions at the input scale $Q_0^2 = 4.0 \text{ GeV}^2$, ISET=2, (solid line) compared to results obtained by GRSV (dashed-dotted line) [16] and AAC (dashed line) [15]. The shaded areas represent the fully correlated 1σ error bands calculated by Gaussian error propagation. The dark dotted lines correspond to the positivity bounds according to the parameterization [27].

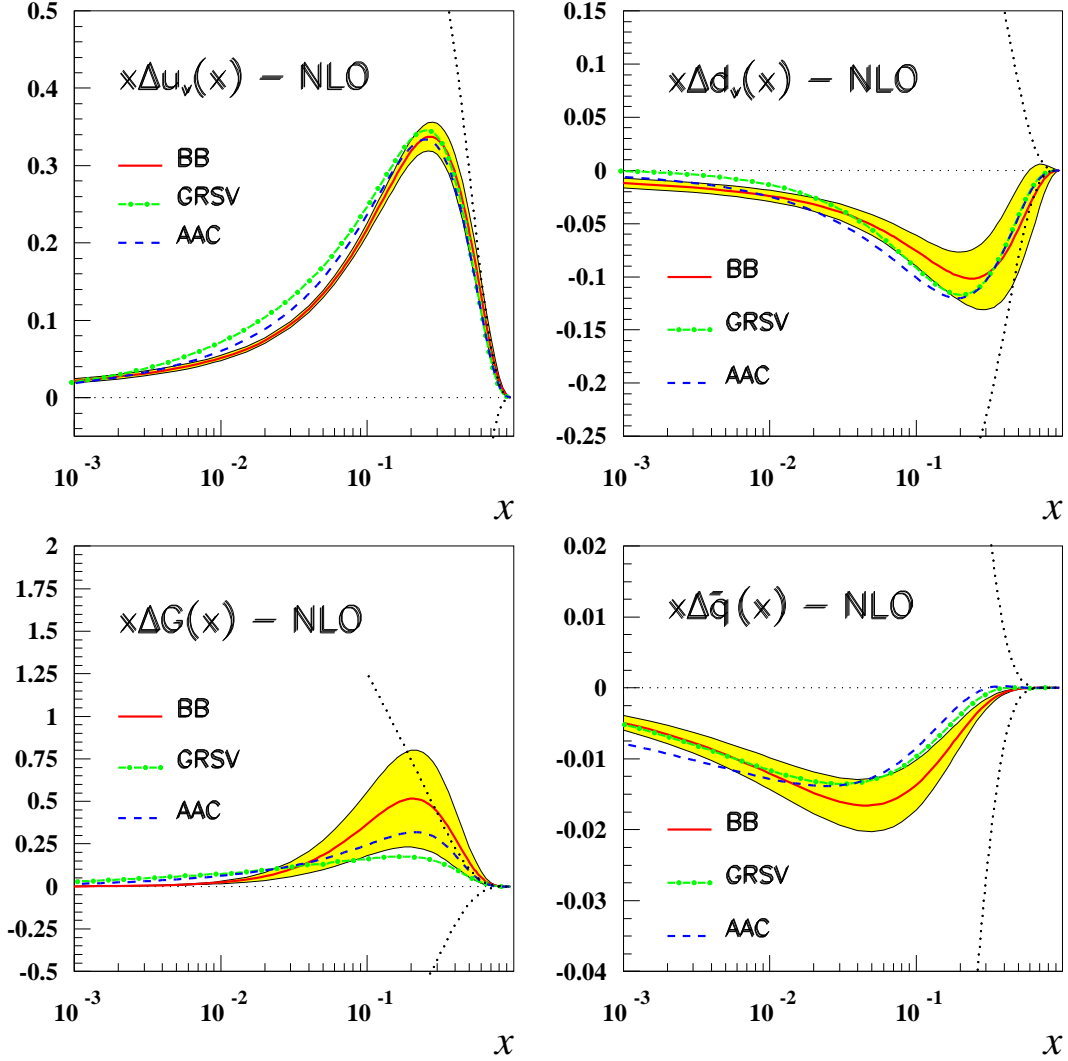


Figure 3: NLO polarized parton distributions at the input scale $Q_0^2 = 4.0 \text{ GeV}^2$, ISET=3, (solid line) compared to results obtained by GRSV (dashed-dotted line) [16] and AAC (dashed line) [15]. The shaded areas represent the fully correlated 1σ error bands calculated by Gaussian error propagation. The dark dotted lines correspond to the positivity bounds choosing [27] for reference.

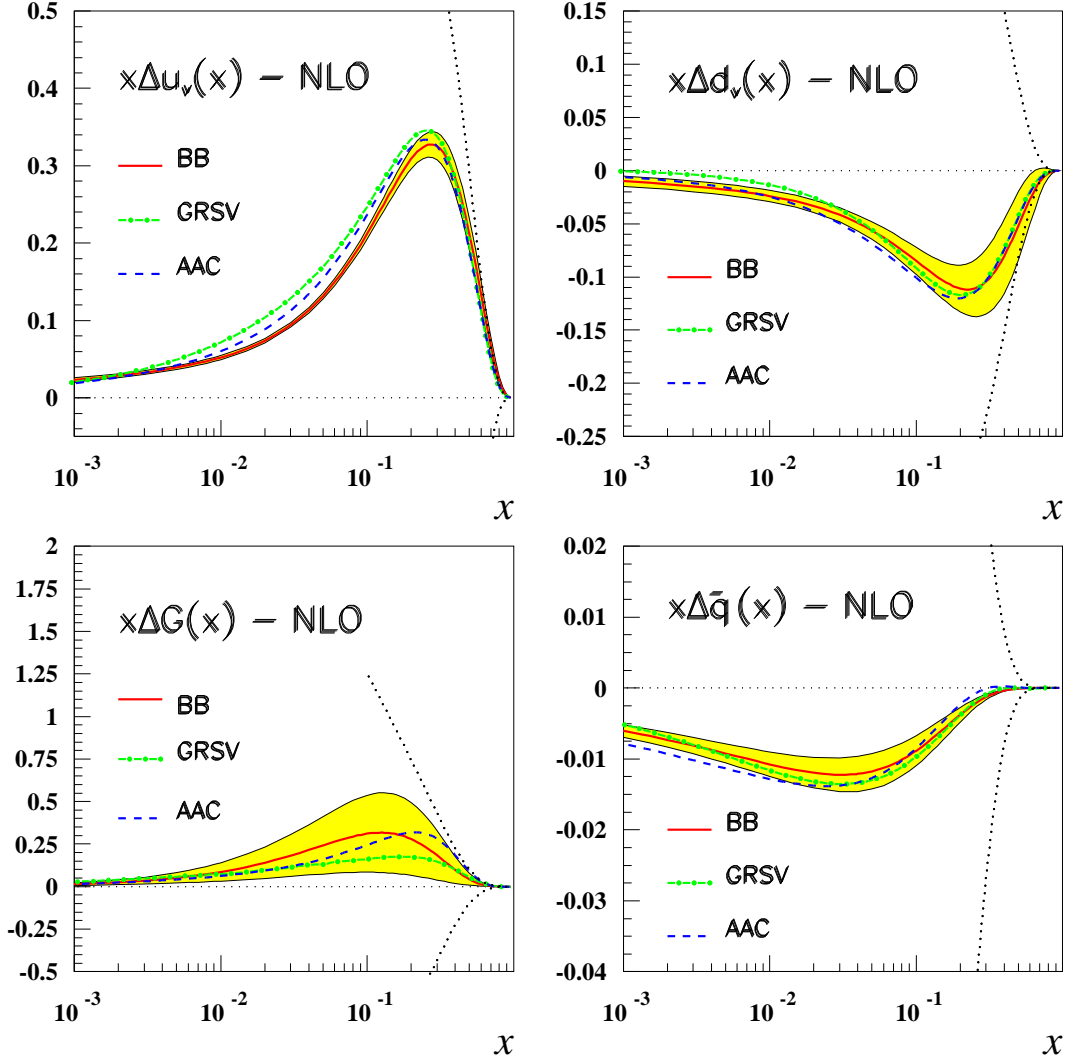


Figure 4: NLO polarized parton distributions at the input scale $Q_0^2 = 4.0 \text{ GeV}^2$, ISET=4, (solid line) compared to results obtained by GRSV (dashed-dotted line) [16] and AAC (dashed line) [15]. The shaded areas represent the fully correlated 1σ error bands calculated by Gaussian error propagation. The dark dotted lines indicate the positivity bound if reference is taken to the distributions [27].

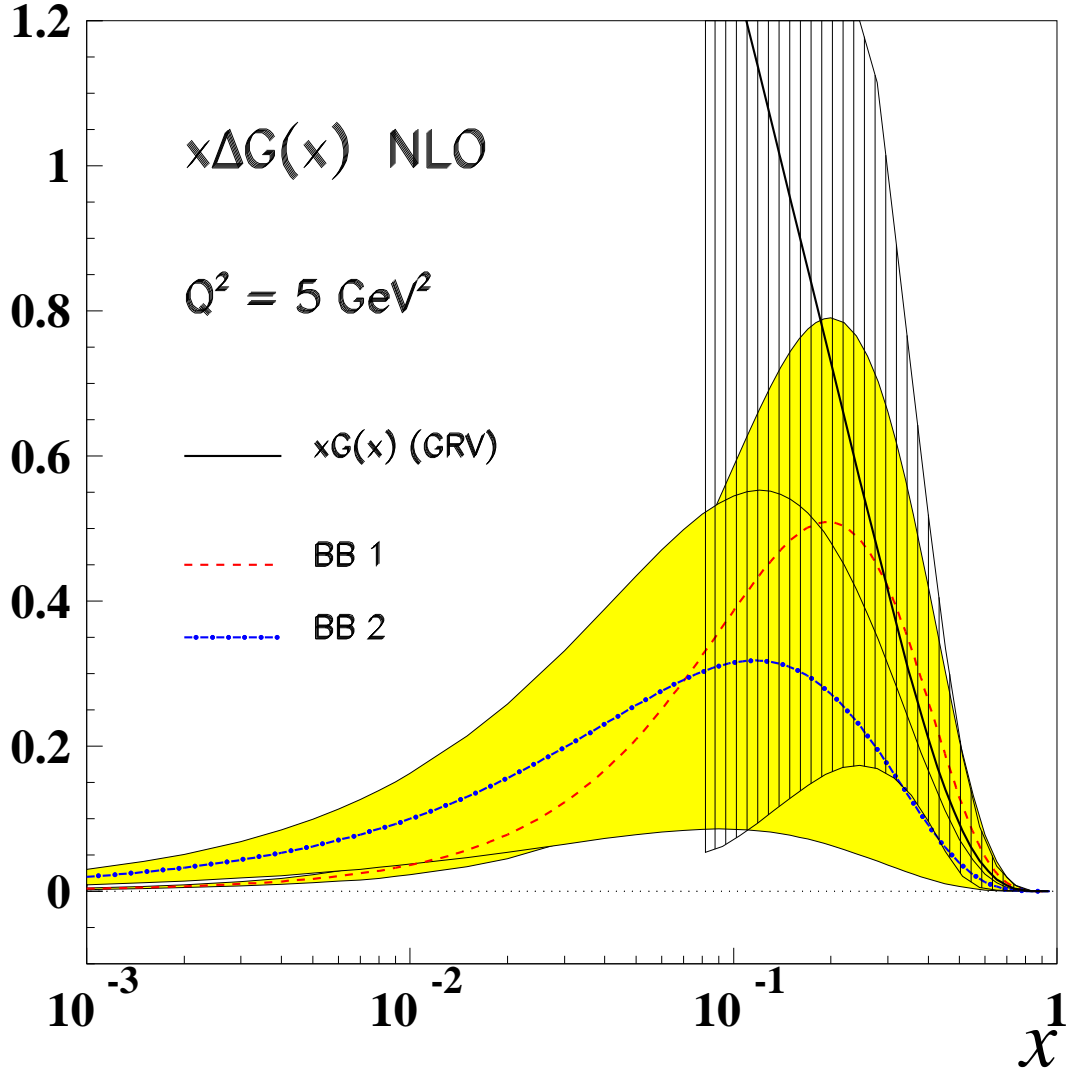


Figure 5: NLO polarized momentum distribution for the gluon at the input scale $Q_0^2 = 5.0 \text{ GeV}^2$ for ISET=3 (BB1, dashed line) and ISET =4 (BB2, dash-dotted line) with 1σ error bands shown (shaded areas). The solid line corresponds to the unpolarized distribution [27]. To the latter we added the experimental error of the unpolarized gluon distribution as determined in the H1 experiment [47] (hatched area), see also [48].

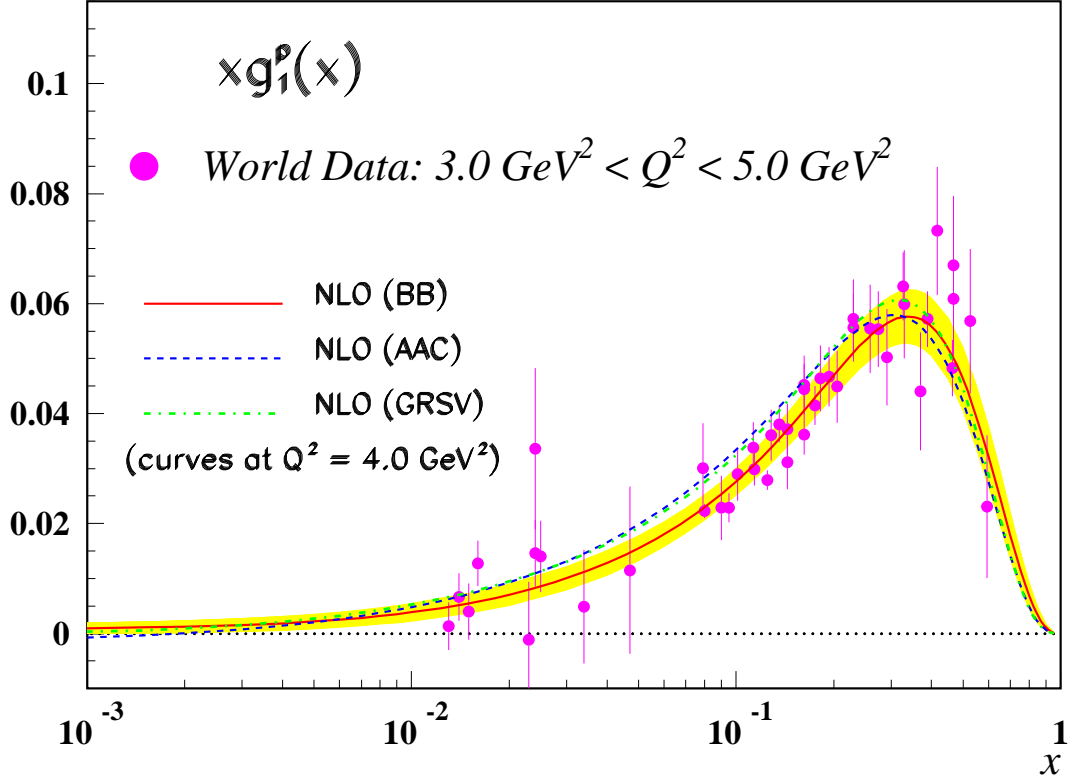


Figure 6: The structure function xg_1^p measured in the interval $3.0 \text{ GeV}^2 < Q^2 < 5.0 \text{ GeV}^2$ as function of x . The structure function $g_1^p(x, Q^2)$ has been derived from the world asymmetry data. The error bars shown are the statistical errors only. The distribution is well described by our QCD NLO curve ISET=3 (solid line) at $Q^2 = 4.0 \text{ GeV}^2$ and its fully correlated 1σ error band calculated by Gaussian error propagation (shaded area). Also shown are the QCD NLO curves at the same value of Q^2 obtained by AAC (dotted line) [15] and GRSV (dashed line) [16] for comparison.

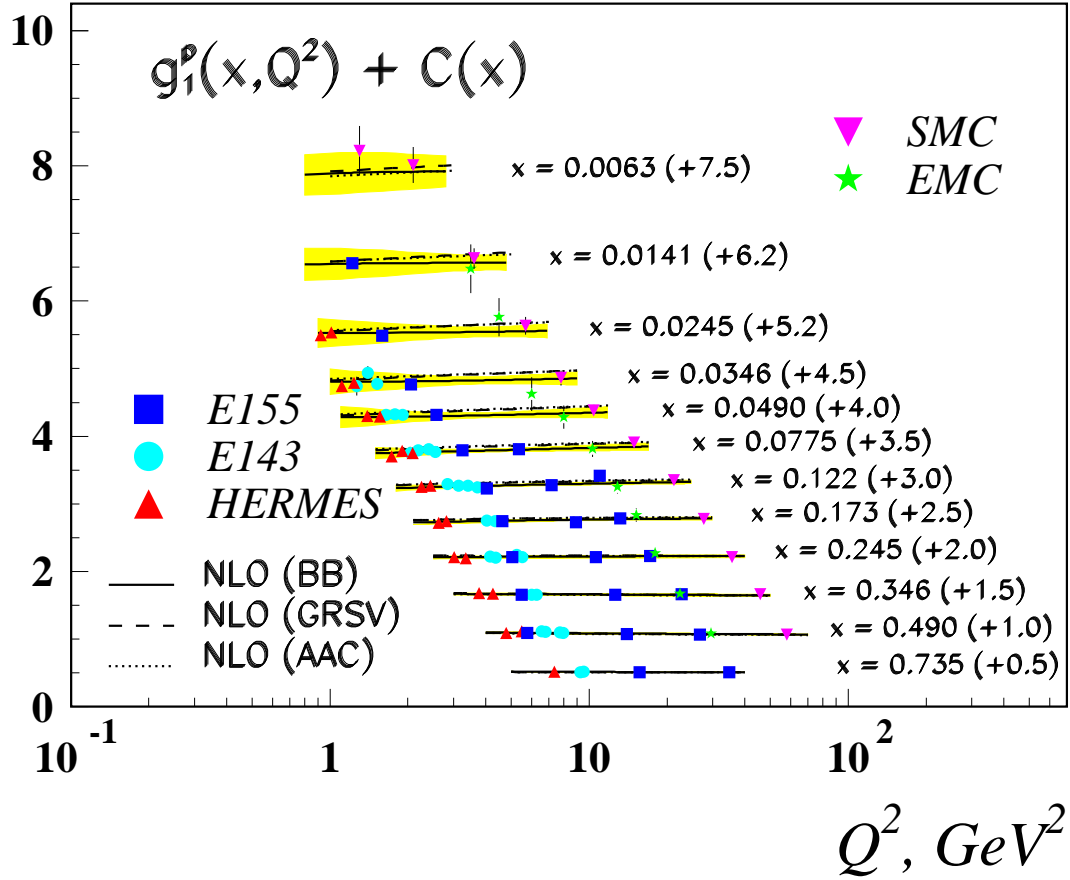


Figure 7: The polarized structure function g_1^p as function of Q^2 in intervals of x . The error bars shown are the statistical and systematic uncertainties added in quadrature. The data are well described by our QCD NLO curves (solid lines), ISET=3, and its fully correlated 1σ error bands calculated by Gaussian error propagation (shaded area). The values of $C(x)$ are given in parentheses. Also shown are the QCD NLO curves obtained by AAC (dashed lines) [15] and GRSV (dashed-dotted lines) [16] for comparison.

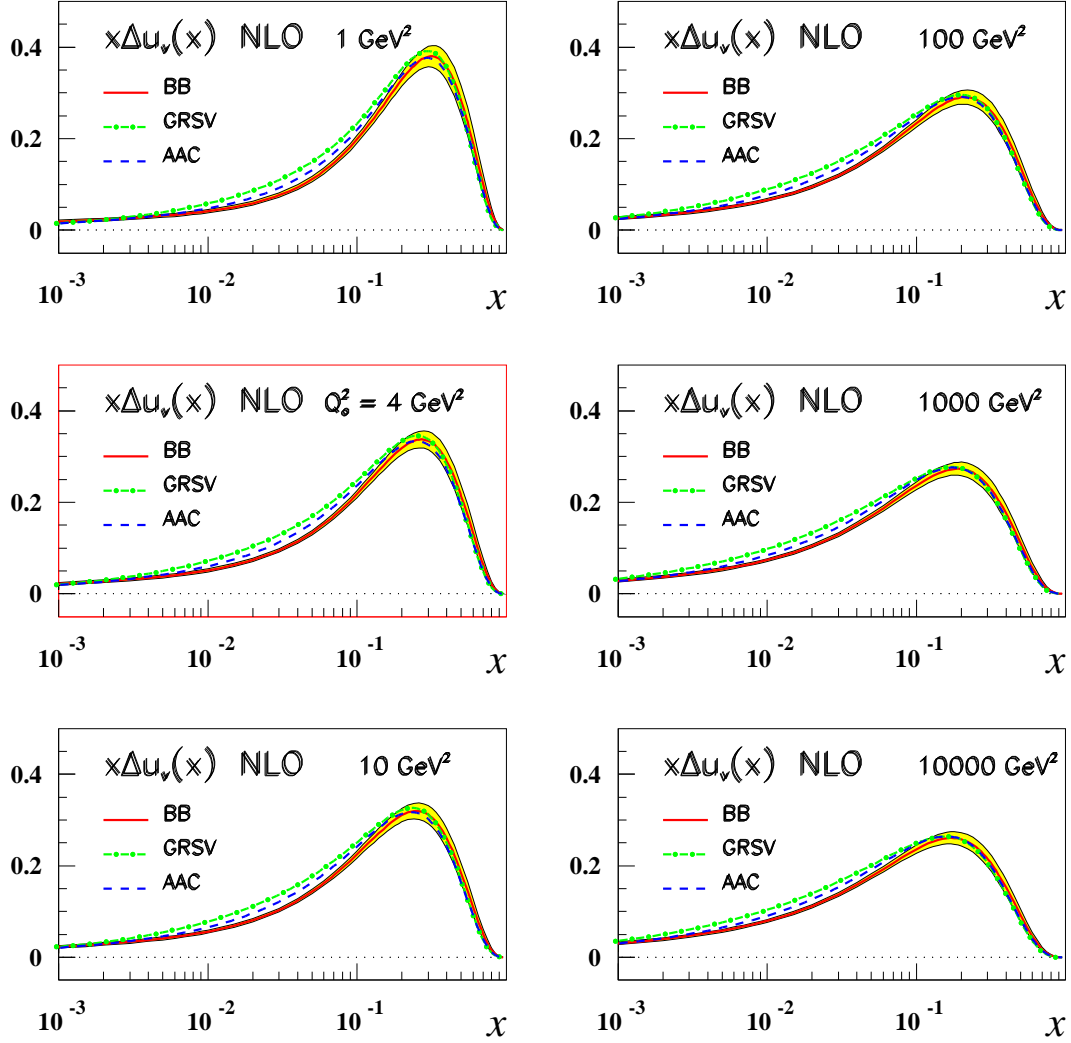


Figure 8: The polarized parton distribution $x\Delta u_v$, ISET=3, evolved up to values of $Q^2 = 10, 100, 1000, 10000 \text{ GeV}^2$ (solid lines) compared to results obtained by GRSV (dashed-dotted lines) [16] and AAC (dashed lines) [15]. The shaded areas represent the fully correlated 1σ error bands from our analysis calculated by Gaussian error propagation.

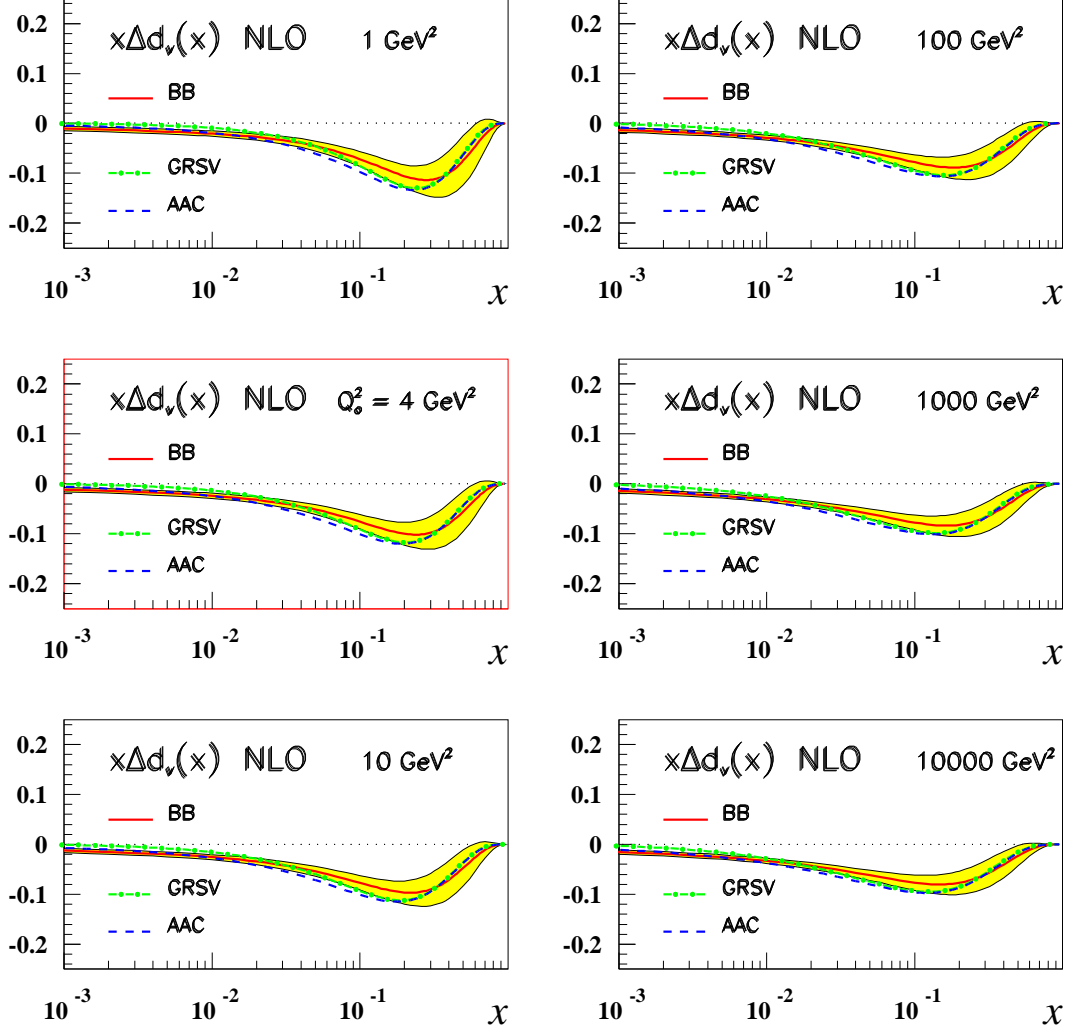


Figure 9: The polarized parton distribution $x\Delta d_v$, ISET = 3, evolved up to values of $Q^2 = 10, 000 \text{ GeV}^2$ (solid lines) compared to results obtained by GRSV (dashed-dotted lines) [16] and AAC (dashed lines) [15]. The shaded areas represent the fully correlated 1σ error bands from our analysis calculated by Gaussian error propagation.

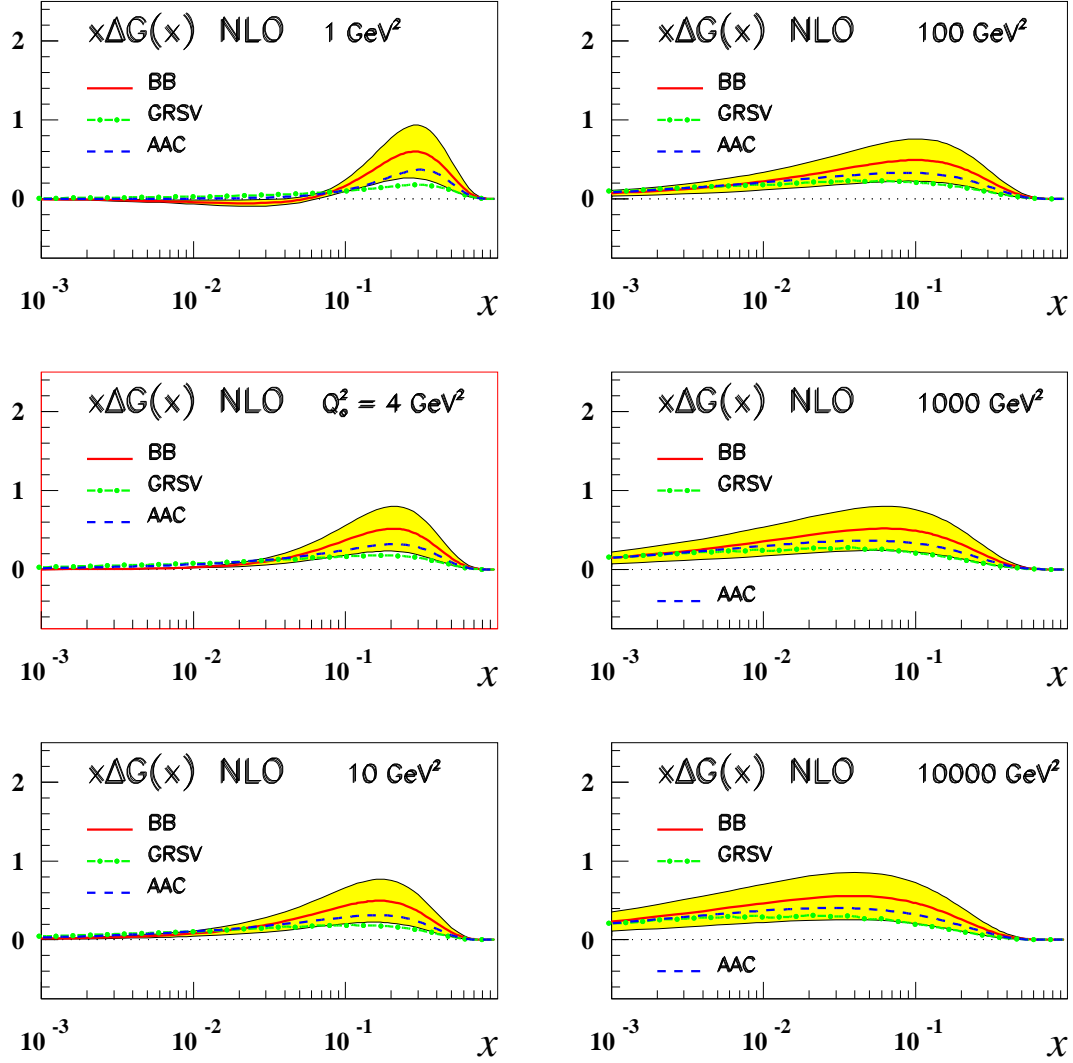


Figure 10: The polarized parton distribution $x\Delta G$, ISET = 3, evolved up to values of $Q^2 = 10, 000 \text{ GeV}^2$ (solid lines) compared to results obtained by GRSV (dashed-dotted lines) [16] and AAC (dashed lines) [15]. The shaded areas represent the fully correlated 1σ error bands from our analysis calculated by Gaussian error propagation.

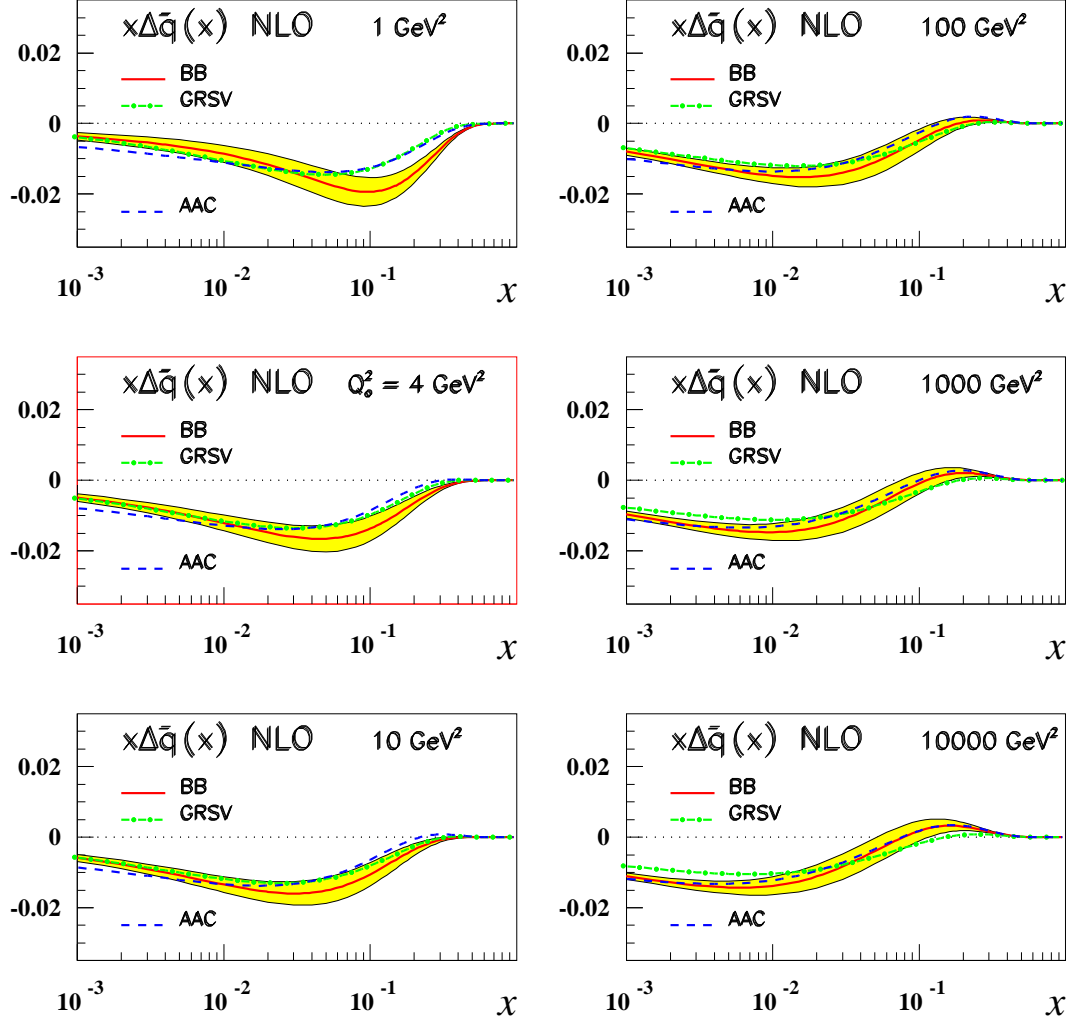


Figure 11: The polarized parton distribution $x\Delta\bar{q}$, ISET =3, evolved up to values of $Q^2 = 10,000 \text{ GeV}^2$ (solid lines) compared to results obtained by GRSV (dashed-dotted lines) [16] and AAC (dashed lines) [15]. The shaded areas represent the fully correlated 1σ error bands from our analysis calculated by Gaussian error propagation.

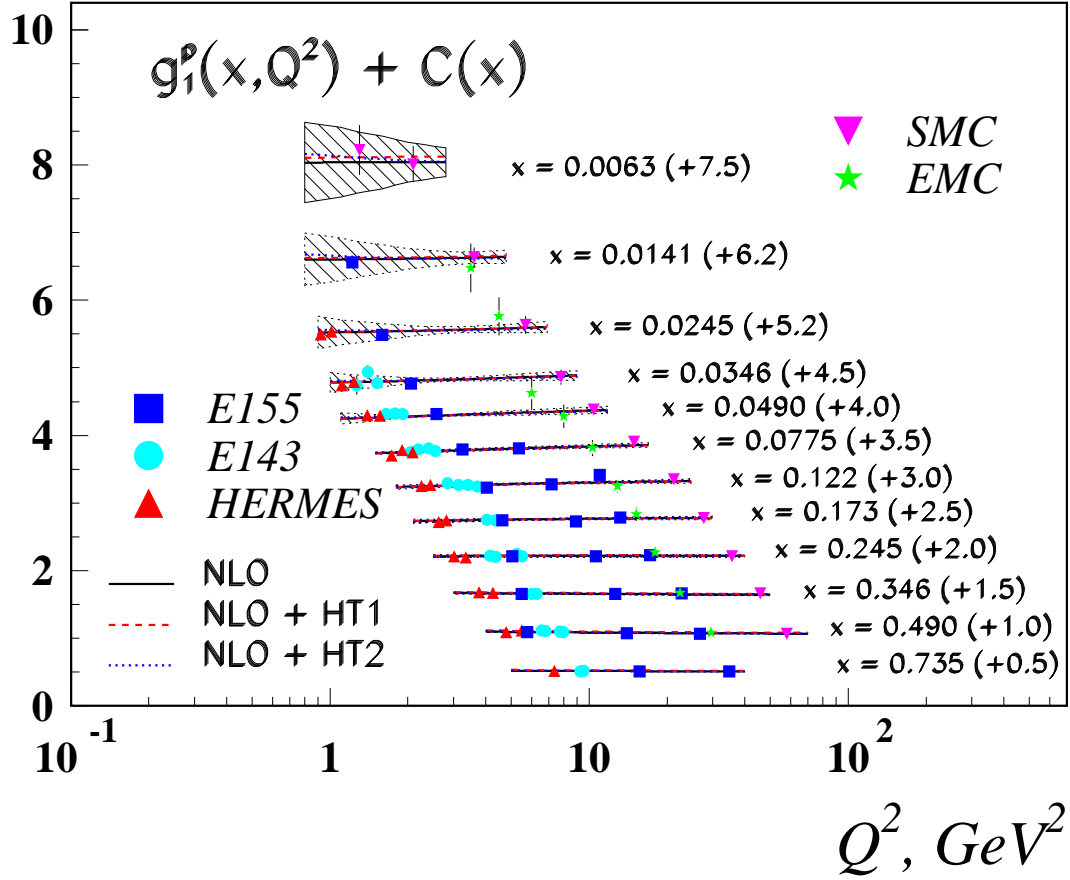


Figure 12: Model fit to potential power corrections in $g_1(x, Q^2)$ as extracted from the world polarization asymmetry data in the present analysis (see text). Dashed line: model I, Eq. (70); dotted line: model II, Eq. (71). The full lines correspond to the parameterization (ISET=4) in the present analysis, to which the corresponding power correction model induces a perturbation. The shaded area corresponds to the 1σ correlated error.

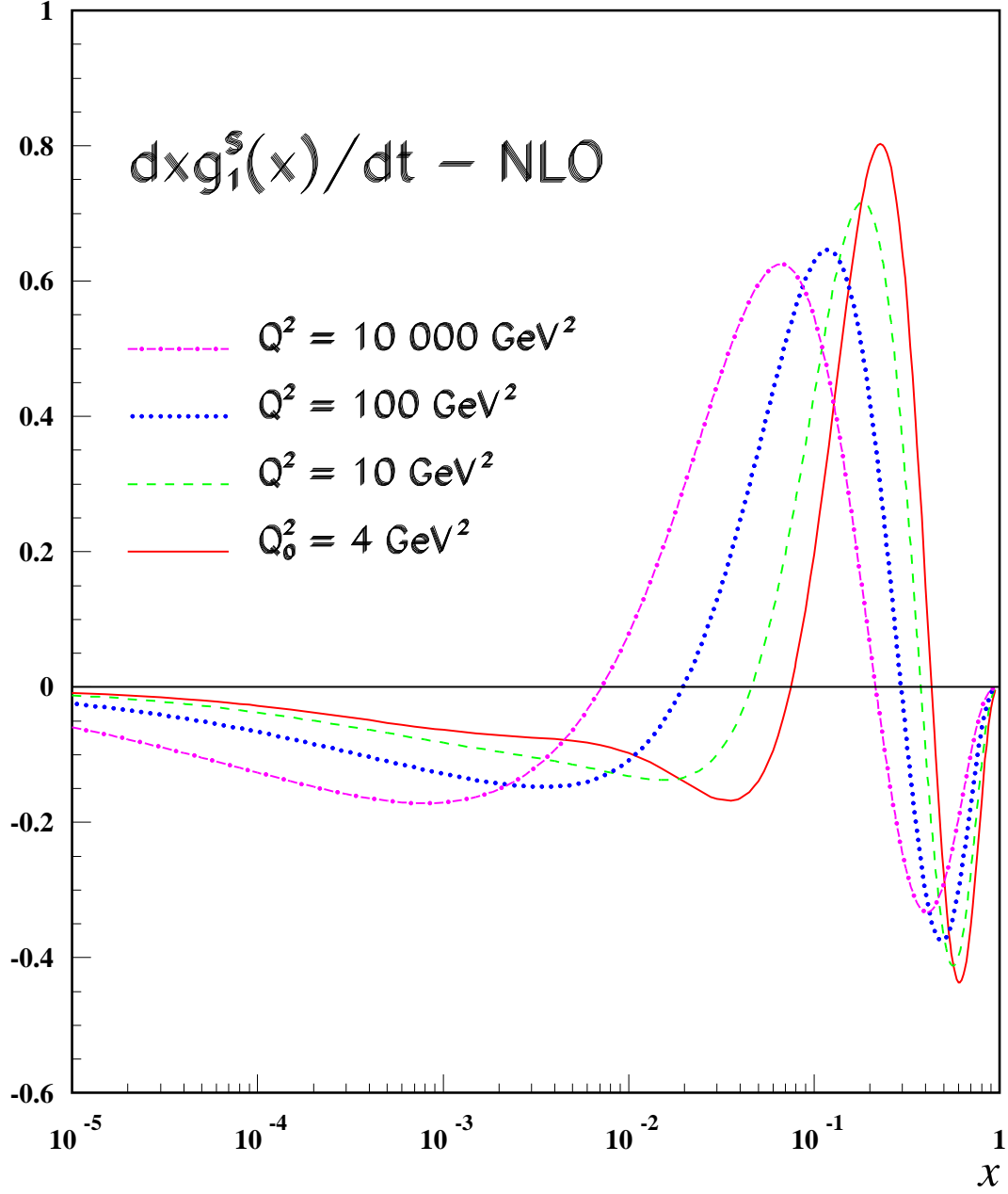


Figure 13: The evolution of $\partial xg_1^S(x, Q^2)/\partial t$, the slope of the polarized structure function $xg_1^p(x, Q^2)$ of the proton (singlet contribution) with respect to $t = -2/\beta_0 \ln(\alpha_s(Q^2)/\alpha_s(Q_0^2))$ [23]. The slope was determined from a fit to $g_1^p(x, Q^2)$, see text.

References

- [1] R. Mertig and W.L. van Neerven, Z. Phys. **C70** (1996) 637,
W. Vogelsang, Phys. Rev. **D54** (1996) 2023.
- [2] see e.g. : W. Furmanski and R. Petronzio, Z. Phys. **C11** (1982) 293 and references therein.
- [3] W.L. van Neerven and E.B. Zijlstra, Nucl.Phys. **B417** (1994) 61, E: **B426** (1994) 245.
- [4] J. Ashman et al., EMC collaboration, Phys. Lett. **B206** (1988) 364; Nucl. Phys. **B328** (1989) 1.
- [5] P.L. Anthony et al., E142, Phys. Rev. **D54** (1996) 6620.
- [6] K. Ackerstaff et al., HERMES collaboration, Phys. Lett. **B404** (1997) 383.
- [7] K. Abe et al., E154, Phys. Rev. Lett. **79** (1997) 26.
- [8] B. Adeva et al., SMC collaboration, Phys. Rev. **D58** (1998) 112001.
- [9] K. Abe et al., E143, Phys. Rev. **D58** (1998) 120003.
- [10] A. Airapetian et al., HERMES collaboration, Phys. Lett. **B442** (1998) 484;
D. Hasch, PhD thesis, Humboldt-Univ. Berlin, (1999) and DESY-THESIS-2000-032.
- [11] P.L. Anthony et al., E155, Phys. Lett. **B463** (1999) 339.
- [12] P.L. Anthony et al., E155, Phys. Lett. **B493** (2000) 19.
- [13] M.J. Alguard et al., E80, Phys. Rev. Lett. **37** (1976) 1261.
G. Baum et al., E130, Phys. Rev. Lett. **51** (1983) 1135.
- [14] G. Altarelli et al., Nucl. Phys. **B496** (1997) 337; Acta Phys. Pol. **B29** (1998) 1145;
S. Forte, M. Mangano, and G. Ridolfi, Nucl. Phys. **B602** (2001) 585.
- [15] Y. Goto et al., AAC collaboration, Phys. Rev. **D62** (2000) 034017.
- [16] M. Glück et al., Phys. Rev.. **D63** (2001) 094005.
- [17] E. Leader, A. Sidorov, and D. Stamenov, hep-ph/0111267.
- [18] H.-Y. Cheng and S.-N. Lai, Phys. Rev. **D41** (1990) 91;
S. Gupta, J. Pasupathy, and J. Szwed, Z. Phys. **C46** (1990) 111;
M. Glück, E. Reya, and W. Vogelsang, Nucl. Phys. **B329** (1990) 347;
P. Chiappetta and G. Nardulli, Z. Phys. **C51** (1991) 435;
K. Sridhar and E. Leader, Phys. Lett. **B295** (1992) 283;
H.-Y. Cheng and C. F. Wai, Phys. Rev. **D46** (1992) 125;
D. de Florian et al., Phys. Lett. **B319** (1993) 285; Phys. Rev. **D51** (1995) 37;
P. Chiappetta et al., Z. Phys. **C59** (1993) 629;
P. Nadolsky, Z. Phys. **C63** (1994) 601;
S.J. Brodsky, M. Burkhardt, and I. Schmidt, Nucl. Phys. **B441** (1995) 197;
C. Bourrely and J. Soffer, Nucl. Phys. **B445** (1995) 341; Phys. Rev. **D51** (1995) 2108;
F. Buccella and J. Soffer, Mod. Phys. Lett. **A8** (1993) 225; Europhys. Lett. **24** (1993) 165;

- Phys. Rev. **D48** (1993) 5456;
 C. Bourrely et al., Z. Phys. **C62** (1994) 431;
 F. Buccella et al., Z. Phys. **C38** (1995) 631; Nuovo Cim. **A109** (1996) 159;
 G. Ladinsky, A collection of polarized parton densities, in: Proc. Workshop on the Prospects of Spin Physics at HERA, DESY 95–200, Eds. J. Blümlein and W.-D. Nowak, pp. 285; [hep-ph/9601287](#);
 J. Blümlein, *ibid.* pp. 179, [hep-ph/9508387](#);
 H.-Y. Cheng, H. H. Liu, and C.-Y. Wu, Phys. Rev. **D53** (1996) 2380;
 T. Gehrmann and W.J. Stirling, Z. Phys. **C75** (1995) 461; Phys. Rev. **D53** (1996) 6100;
 R. Ball, S. Forte, and G. Ridolfi, Nucl. Phys. **B444** (1995) 287; Phys. Lett. **B378** (1996) 255;
 M. Glück et al., Phys. Rev. **D53** (1996) 4775;
 D. de Florian, O. Sampayo, and R. Sassot, Phys. Rev. **D57** (1998) 5803;
 L.E. Gordon, M. Goshtasbpour, and G.P. Ramsey, Phys. Rev. **D58** (1998) 094017;
 D. Ghosh, S. Gupta, D. Indumathi, Phys. Rev. **D62** (2000) 094012. C. Bourrely, J. Soffer, and F. Buccella, [hep-ph/0109160](#), Eur. Phys. J. **C** in print.
- [19] M. Glück and E. Reya, [hep-ph/0203063](#);
 HERMES collaboration, in preparation.
- [20] J. Blümlein and A. Vogt, Phys. Lett. **B381** (1996) 296; **B386** (1996) 350; Acta Phys. Pol. **B28** (1997) 577;
 J. Bartels, B. Ermolaev, and M. Ryskin, Z. Phys. **C72** (1996) 627;
 Y. Kiyo, J. Kodaira, and H. Tochimura, Z. Phys. **C74** (1997) 631;
 J. Blümlein and A. Vogt, Phys. Rev. **D57** (1998) R1;
 J. Blümlein and W.L. van Neerven, Phys. Lett. **B450** (1999) 412;
 J. Blümlein, V. Ravindran, W.L. van Neerven, and A. Vogt, [hep-ph/9806368](#), in: Proceedings of DIS98, Brussels, eds. Gh. Coremans and R. Rosen, (World Scientific, Singapore, 1998), pp. 216;
 J. Blümlein, in: Proc. Ringberg Workshop: New Trends in HERA Physics, Lecture Notes in Physics **Vol. 546** (Springer, Berlin, 2000), pp. 42, [hep-ph/9909449](#).
- [21] J. Blümlein and A. Vogt, Phys. Rev. **D58** (1998) 014020.
- [22] G. Altarelli and G. Ross, Phys. Lett. **B212** (1988) 391;
 G. Altarelli and B. Lampe, Z. Phys. **C47** (1990) 315;
 A. Efremov, and O.Teryaev, Dubna preprint E2-88-287;
 R.D. Carlitz, J.C. Collins and A.H. Mueller, Phys. Lett. **B214** (1988) 229.
- [23] J. Blümlein, V. Ravindran, and W.L. van Neerven, Nucl. Phys. **B586** (2000) 349; Acta Phys. Pol. **B29** (1998) 2581; [hep-ph/0101235](#).
- [24] M. Göckeler et al., QCDSF collaboration, Phys. Rev. **D53** (1996) 2317; Phys. Lett. **B414** (1997) 340; [hep-ph/9711245](#); Phys. Rev. **D63** (2001) 074506;
 S. Capitani et al., Nucl. Phys. (Proc. Suppl.) **B79** (1999) 548.
- [25] S. Güsken et al., SESAM collaboration, [hep-lat/9901009](#).
- [26] D. Dolgov et al., LHPC and SESAM collaborations, [hep-lat/0201021](#).

- [27] M. Glück, E. Reya, and A. Vogt, Z. Phys. **C48** (1990) 471.
- [28] M. Glück and E. Reya, Phys. Rev. **D25** (1982) 1211;
G. Grunberg, Phys. Rev. **D29** (1984) 2315;
S. Catani, Z. Phys. **C75** (1997) 665;
R. Thorne, Nucl. Phys. **B512** (1998) 323;
J. Blümlein and A. Vogt, unpublished.
- [29] L. Baulieu and C. Kounnas, Nucl. Phys. **B155** (1979) 429.
- [30] J. Blümlein and S. Kurth, [hep-ph/9708388](#); Phys. Rev. **D60** (1999) 014018;
J. Vermaseren, Int. J. Mod. Phys. **A14** (1999) 2037;
J. Blümlein, [hep-ph/003100](#), Comp. Phys. Commun. **133** (2000) 76.
- [31] W.L. van Neerven and A. Vogt, Phys. Lett. **B490** (2000) 111.
- [32] I. Akushevich et al., Acta. Phys. Pol. **B28** (1997) 563.
- [33] D. Bardin, J. Blümlein, O. Christova, and L. Kalinovskaya, Nucl. Phys. **B506** (1997) 295;
[hep-ph/9609399](#);
D. Bardin et al., Acta Phys. Pol. **B28** (1997) 511;
A. Arbuzov et al., Comput. Phys. Commun. **94** (1996) 128;
J. Blümlein and H. Kawamura, DESY 02–16.
- [34] L.W. Withlow et al., Phys. Lett **B250** (1990) 193.
- [35] M. Arneodo et al., NMC collaboration, Nucl. Phys. **B483** (1997) 3.
- [36] K. Abe et al., E143, Phys. Lett. **B452** (1999) 194.
- [37] D. Adams et al., SMC collaboration, Phys. Lett. **B336** (1994) 125.
- [38] K. Abe et al. (E154)), Phys. Lett. **B404** (1997) 377.
- [39] S. Wandzura, F. Wilczek, Phys. Lett. **B72** (1977) 195.
- [40] J. Blümlein and A. Tkabladze, Nucl. Phys. **B553** (1999) 427; Nucl. Phys. **B** (Proc. Suppl.) **79** (1999) 427.
- [41] A. Piccione and G. Ridolfi, Nucl. Phys. Nucl. Phys. **B513** (1998) 301.
- [42] J. Blümlein and N. Kochelev, Phys. Lett. **B381** (1996) 296; Nucl. Phys. **B498** (1997) 285.
- [43] J. Blümlein and D. Robaschik, Phys. Lett. **B517** (2001) 222; [hep-ph/0202077](#).
- [44] M. Arneodo et al. (NMC), Phys. Lett. **B364** (1995) 107.
- [45] F. James, CERN Program Library, Long Writeup D506.
- [46] M. Glück, E. Reya, and A. Vogt, Eur. Phys. J. **C5** (1998) 461.
- [47] C. Adloff et al., H1 collaboration, Eur. Phys. J. **C21** (2001) 33.
- [48] J. Pumplin et al, CTEQ group, [hep-ph/0201195](#).

- [49] Particle Data Group, Eur. Phys. J. **C3** (1998) 1.
- [50] G. Altarelli, S. Forte, and G. Ridolfi, Nucl. Phys. **B543** (1998) 277.
- [51] K. Abe et al. (E154), Phys. Lett. **B405** (1997) 180.
- [52] B. Adeva et al. (SMC), Phys. Rev. **D58** (1998) 112002.
- [53] Particle Data Group, Eur. Phys. J. **C15** (2000) 91.
- [54] J. Blümlein, V. Ravindran, J. Ruan, and W. Zhu, Phys. Lett. **B504** (2001) 235.
- [55] For discussions see contributions to DIS92, Proceedings of the 1992 Zeuthen Workshop on Elementary Particle Theory, **Deep Inelastic Scattering**, eds. J. Blümlein and T. Riemann, Nucl. Phys. **B** (Proc. Suppl.) **29A**.